

Improved modelling of mountain snowpacks with spatially distributed precipitation bias correction derived from historical reanalysis

Manon von Kaenel¹, Steven A. Margulis¹

5 ¹Civil and Environmental Engineering, University of California Los Angeles, Los Angeles, 90095, USA

Correspondence to: Manon von Kaenel (mvonkaenel@g.ucla.edu)

Abstract. Accurate estimates of snow water equivalent (SWE) are essential for effective water management in regions dependent on seasonal snowmelt. However, significant biases and high uncertainty in mountain precipitation data products pose significant challenges. This study leverages a SWE reanalysis framework and historical dataset to derive factors that can

10 downscale and bias-correct mountain precipitation in a real-time modelling context. We evaluate through hindcast modelling how different versions of this precipitation bias correction affect errors in 1 April SWE estimates within a representative snow-dominated watershed in the Western U.S. We also evaluate how the additional assimilation of fractional snow-covered area (fSCA) or snow depth observations during the accumulation season impact the 1 April SWE estimates. Results show that

15 spatially distributed historically informed precipitation bias correction significantly improves SWE estimates, reducing the multi-year averaged normalized root mean square difference (NRMSD) from 78% to 33% (-58%), increasing the correlation (R) from 0.63 to 0.9 (+43%), and decreasing mean difference (MD) from -340 mm to -41 mm (-88%). The primary strength of this bias correction method lies in capturing the spatial distribution of precipitation bias rather than its interannual variability.

20 Assimilating snow depth observations further reduces errors both at the watershed scale (NRMSD less by 46%) and pixel level in most years, while, as expected, accumulation season fSCA assimilation is not generally useful. We demonstrate the value of these methods for streamflow forecasts: bias-corrected precipitation improves the correlation between daily simulated snowmelt and observed streamflow by 31-39% and reduces bias in predicted April-July runoff volumes by 46-52%. This study highlights how historical SWE reanalysis datasets can be leveraged and applied in a real-time context by informing precipitation bias correction.

1 Introduction

25 Seasonal snowpack is a natural water tower; by storing winter precipitation and releasing it as snowmelt, it provides an essential resource for downstream ecosystems and an estimated 20% of the Earth's population (Dozier, 2011). In order to make critical management decisions for flood control, hydropower operations, irrigation, and other competing demands in snow-dependent regions of the world, water managers need accurate assessments of the distribution and availability of water in snowpack (e.g., Hamlet et al., 2002; Koster et al., 2010; He et al., 2016). Estimating the spatiotemporal distribution and

30 change of snow water equivalent (SWE) remains a significant and important challenge for the snow hydrology community (e.g., Cho et al., 2022; Dozier et al., 2016; Lettenmaier et al., 2015).

35 Large-scale and temporally continuous SWE measurements are generally absent from the real-time observational record. In situ data from networks such as the Western U.S. SNOTEL (snow telemetry) network are not always representative of the heterogeneity of SWE distribution in topographically complex mountain landscapes (e.g., Herbert et al., 2024), and such networks are sparse globally. For example, although seasonal snowpack is crucial to local water availability in High Mountain Asia, the region has almost no in situ data (e.g., Liu et al., 2021). Remote sensing can provide measurements of snow properties like fractional snow-covered area (fSCA, e.g., Selkowitz et al., 2017), snow depth (e.g., Painter et al., 2016), or albedo (e.g., Bair et al., 2019) over large areas, but there is currently no reliable way of measuring SWE from spaceborne platforms particularly in mountainous terrain (Lettenmaier et al., 2015).

40 This implies a continued need for modelling of mountain SWE. Land surface models are commonly used to estimate SWE and other hydrologic variables over large spatial extents (Cho et al., 2022; Clark et al., 2011; Kumar et al., 2013), but these are susceptible to uncertainties driven by biases in forcing data or model parameterization (Cho et al., 2022). Uncertainty in precipitation products in mountainous terrain, and its implications for SWE and downstream hydrology modelling, is a widely acknowledged challenge (e.g., Schreiner-McGraw et al., 2020; Cho et al., 2022; Pan et al., 2003; Raleigh et al., 2015; 45 Liu and Margulis, 2019). Fang et al. (2023) found that the uncertainty of SWE estimates from commonly used global and regional modelling products is primarily explained by precipitation uncertainty. Dynamical and statistical downscaling are two fundamental techniques that translate coarse-scale gridded meteorology to a finer-scale resolution for input to a regional hydrologic model. Statistical downscaling, the less computationally expensive and more common method of the two, relates coarse meteorology fields to high-resolution reference variables and oftentimes inherently includes bias correction (e.g., 50 Gutmann et al., 2014). Recent studies have developed and demonstrated effective machine learning based or statistical downscaling approaches for resolving and/or bias-correcting precipitation fields from satellite-based products (e.g., Sharifi et al., 2019; Lober et al., 2023; Chen et al., 2022; Wang et al., 2023; Zhao 2021; Lu et al., 2020; Ma et al., 2018) and regional climate simulations (e.g., Lie et al., 2021; Velasquez et al., 2020; Yoshikane et al., 2023) in mountainous and moderate-topography regions.

55 Data assimilation has gained popularity as a way to constrain or correct uncertain model estimates of snow with observations of variables such as fSCA or snow depth, and has demonstrated ability as a method to quantify SWE over both melt and accumulation seasons (Magnusson et al., 2014; Margulis et al., 2016; Cortes et al., 2016; Langeron et al., 2020; Liu et al., 2021; Fang et al., 2022; Alonso-González et al., 2022; Aalstad et al., 2018). This approach is particularly valuable in regions where in situ data are sparse but remotely sensed observations like fSCA are available, such as High Mountain Asia 60 (Liu et al., 2021) or the South American Andes (Cortes et al., 2016). However, such products are typically only generated retrospectively. Recent studies have shown promise in combining historical reanalysis snow estimates with in situ and/or remotely sensed snow observations using statistical methods to specifically develop near real-time SWE estimates (Pflug et al., 2022; Schneider and Molotch, 2016; Bair et al., 2018; Zheng et al., 2018; Yang et al., 2022). While these methods still

heavily rely on ground SWE observations, they do demonstrate the value of and potential for historical reanalysis SWE datasets
65 to inform SWE estimation in an operational context.

Real-time spatially distributed SWE estimates have significant potential for application to water management. Climate change impacts in snow-influenced systems, such as earlier runoff of snowmelt and drops in snowpack volume, pose important challenges for water managers (e.g., Berg and Hall, 2017). Accurate and timely seasonal streamflow forecasts help inform management decisions that allocate resources in a way that is resilient to climate variability or drought (e.g., Tanaka et
70 al., 2006). Ensemble streamflow prediction (ESP) uses hydrologic models to forecast future streamflow from current snow, soil moisture, river and reservoir conditions (Wood et al., 2002). The skill of these model-based streamflow forecasts is primarily derived from initial SWE and soil moisture conditions (Koster et al., 2010). This suggests that accurate spatially continuous real-time SWE estimates could be used to reduce uncertainty and error in streamflow forecasts in snow-dominated regions.

75 Reanalysis methods that incorporate satellite-based observations have demonstrated effectiveness in estimating SWE retrospectively over areas where in situ data is sparse, but producing accurate precipitation fields remains a challenge and a need for modeling snow in mountainous regions. In this paper we leverage a SWE reanalysis framework and historical dataset to address this gap and gain insight into how to improve modeling. Specifically, we derive mountain precipitation bias correction estimates, and develop and test spatially continuous SWE estimates on 1 April. The motivating questions are: 1) To
80 what extent can historically informed mountain precipitation bias correction improve model-based spatial SWE estimates? 2) How does the assimilation of accumulation season fSCA and snow depth measurements into this framework affect those estimates? 3) How are snowmelt-driven streamflow predictions affected under these scenarios? We validate these methods over a well-documented study domain, with the potential to extend to areas that have less access to in situ data.

2 Methods

85 2.1 Study domain

The study domain comprises the Hetch Hetchy watershed, a headwater catchment for the Tuolumne River in the California Sierra Nevada (Fig. 1). Its drainage area ($\sim 1,200 \text{ km}^2$) is characterized by complex topography with elevations ranging from 1,150 m to 3,850 m. The watershed is part of Yosemite National Park, which according to the National Park Service receives 95% of its precipitation between October and May, and 75% of that between November and March. During
90 these winter months, temperatures at high alpine watersheds like the study domain typically average below freezing, and snow covers the ground. Snowmelt occurs in the spring and generates water supply that is stored in the downstream reservoir. It is representative of other snow-dominated catchments that provide key water supply in the Sierra Nevada. More broadly, it is a demonstrative basin that represents global mountain watersheds where the tested methods could provide utility for water management purposes; that is, basins with complex terrain at high elevations and seasonal snowpack that play a significant
95 role in the water budget.

The Hetch Hetchy reservoir at the watershed's outlet provides water supply for about 2.7 million residents of the San Francisco Bay Area, primarily from snowmelt. This watershed also includes a unique Airborne Snow Observatory (ASO) snow depth dataset (Painter et al., 2016) which provides multitemporal lidar-derived snow depth measurements per year. A subwatershed that drains through the USGS TGC (Tuolumne River at Grand Canyon) gauge located at the inlet of the reservoir 100 was delineated for the streamflow analysis.

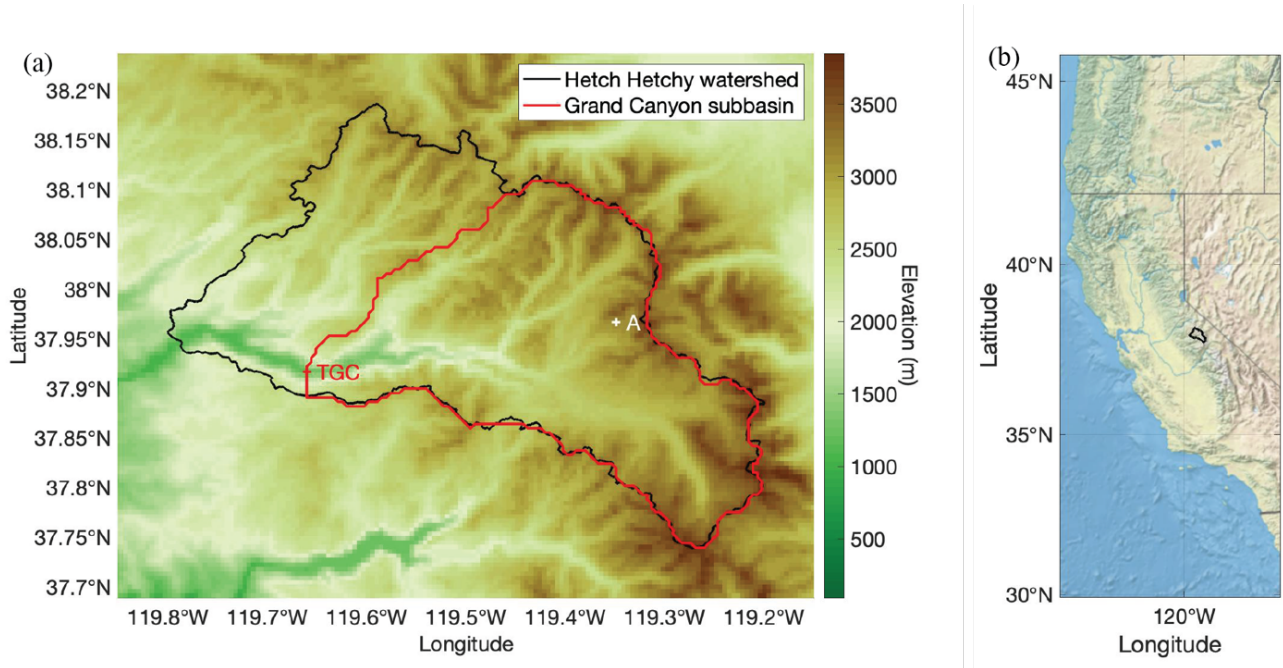


Figure 1. (a) A map outlining the Hetch Hetchy and the Grand Canyon subwatersheds of the Tuolumne River. The locations of the TGC streamflow gauge and sample model pixel A. (b) Outline of the Hetch Hetchy watershed illustrating its location in the central California Sierra Nevada.

105 2.2 Overview of SWE reanalysis framework

A Bayesian reanalysis framework (Margulis et al., 2015) is used in this study for both the development of a historical reference SWE dataset, the derivation of historical precipitation bias correction through retrospective analysis, and testing “real-time” applications using that historical data (along with other data). Note that we use a hindcasting approach to model the real-time applications. The overall methodology is visualized in a flowchart in Fig. 2. Details of the application of this 110 framework in a historical context is in section 2.3 and in a real-time context in section 2.4; here, we provide a general overview of the reanalysis method and its previous applications.

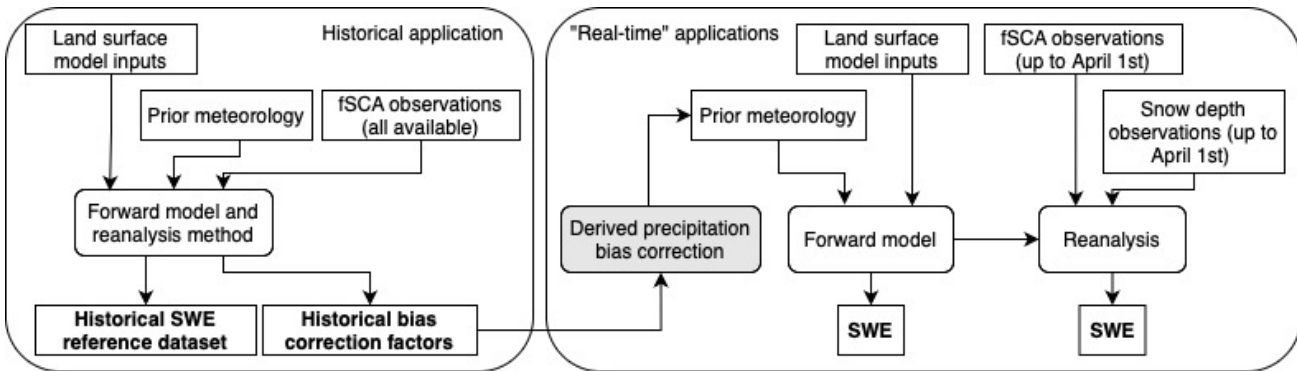


Figure 2. Flowchart illustrating the overall methodology, including inputs, modelling components, and key outputs used for both the historical and real-time applications of the reanalysis framework.

115 Typically applied retrospectively, this reanalysis framework generates spatiotemporally continuous SWE estimates using a particle batch smoother (PBS) data assimilation technique that constrains a prior ensemble of modeled snow estimates with independent observations (most commonly, satellite-based fSCA measurements). The method was developed by Margulis et al. (2015) and has since demonstrated ability to reproduce observed SWE across global mountain regions: Sierra Nevada (Margulis et al., 2016), South American Andes (Cortes et al., 2016), High Mountain Asia (Liu et al., 2021) and the Western 120 U.S. (Fang et al., 2022). It has also demonstrated success in assimilating remotely-sensed snow depth measurements for SWE estimation (Margulis et al., 2019).

125 First, an ensemble of prior snow estimates is generated using a forward land surface model (LSM); here, the modelling core is the SSiB-SAST LSM (Simplified Simple Biosphere - Snow-Atmosphere-Soil Transfer; Sun and Xue, 2001; Xue et al., 2003) paired with the Liston Snow Depletion Curve (Liston 2004). This LSM is driven by meteorological forcings which each explicitly incorporate some measure of a priori bias and uncertainty. Further details on these uncertainty estimates and the modelling approach are in Text S1. Note that implicit in this SWE estimation is the assumption that precipitation (snowfall) in mountainous regions is the largest source of error in the modelling of SWE. Precipitation fields from raw products like MERRA2 tend be coarse, smooth, and biased (Liu and Margulis, 2019; Fig. 3a, b). This is acknowledged by the bias correction and large uncertainty in the postulated prior precipitation distribution, represented by:

$$130 \quad P_j^-(t) = b_j^- * P_{nom}(t) \quad (1)$$

where $P_j^-(t)$ is the prior precipitation value for ensemble j at time step t , P_{nom} is the nominal precipitation estimate (i.e., interpolated from MERRA2 as in Fig. 3b), and b_j^- is a scaling factor where the " $-$ " superscript represents that this is a prior estimate not conditioned on independent observations. The ensemble of scaling factors b (Margulis et al., 2019) are effectively seasonal multiplicative bias correction factors for precipitation. The prior b values are prescribed as a lognormally distributed 135 multiplicative factor that describes first-order bias and uncertainty in the nominal precipitation.

Second, a reanalysis step incorporates independent measurements such as fSCA using a Bayesian PBS update. The a priori (equal) prior weights assigned to each ensemble member are updated to posterior weights that reflect the likelihood that

the ensemble member fits the assimilated measurements. These posterior weights are applied to prior ensemble estimates of SWE to derive posterior estimates. Note that fSCA and other potential measurements used for assimilation are connected based on physical processes in the model to other snow variables such as SWE; thus, the whole suite of snow variables is updated both before and after the assimilated measurement time step. So, although this framework has mainly been used to derive posterior SWE estimates, a by-product of this is posterior estimates of all snow states/fluxes and variables like b described above.

2.3 Development of historical reference dataset and precipitation bias correction

To generate the historical reference SWE dataset for this study, the SWE reanalysis framework was applied to the study domain in the same way as in Fang et al., 2022, but with an increased ensemble size (100) and initial conditions set to default values (for SWE, that value is 0) to focus on the derivation of posterior b values for testing herein (Fig. 2). Forcings were sourced from hourly MERRA2 near-surface meteorological forcing data, and the uncertainty models used to perturb input air temperature, precipitation, dew point temperature, and shortwave radiation, as well as model parameters, use the values derived for the Western U.S. domain by Fang et al. (2022) following the methods outlined in Liu and Margulis (2019) and Girotto et al (2014) (Text S1). For prior precipitation, this uncertainty is quantified by a lognormal distribution of b with nominal mean of 1.8, CV of 0.69, and range of 0.1 to 5 (Fang et al., 2022). The coarse-resolution MERRA2 forcings ($0.5^\circ \times 0.625^\circ$) are first bilinearly interpolated to the model grid resolution (16 arcseconds or ~ 500 m), as is done in the original reanalysis methodology (Fang et al., 2022) (Fig. 3b). Here, we assume that downscaling the prior precipitation to the grid resolution is not known or easily postulated before the reanalysis methodology is applied.

Measurements from Landsat-derived fSCA (raw resolution of ~ 30 m aggregated to modelling resolution) provide the data assimilated into the historical reference dataset. We apply screening methods consistent with Fang et al. (2022) to exclude Landsat observations with cloud cover fraction greater than 40% and individual cloudy pixels with an internal cloud mask. All remaining fSCA measurements are assimilated into the reanalysis retrospectively and as a batch for each water year. A measurement error standard deviation for retrieved Landsat fSCA is specified as 10% (Fang et al., 2022). A uniform spatial resolution of 16 arcseconds (~ 500 m) is chosen, with hourly outputs aggregated to a daily timestep for water years (WYs) 1985 to 2021. Initial conditions are set to default values at the start of each water year; for SWE, that value is 0. This assumes that the seasonal snowpack melts out yearly; although this may not happen every year especially at high-elevation shaded areas of the watershed, we argue this is an assumption worth making to avoid accumulating error and to make fair and consistent comparisons between simulations.

The performance of a similar application of this reanalysis framework is evaluated against independent snow observations in Fang et al. (2022); this verification shows high correlation (0.81 to 0.91) with ASO SWE in the Tuolumne basin (which encompasses the study domain); and good correspondence with in situ SWE in California (root mean square difference = 0.3 m, mean difference = -0.15 m, correlation = 0.82).

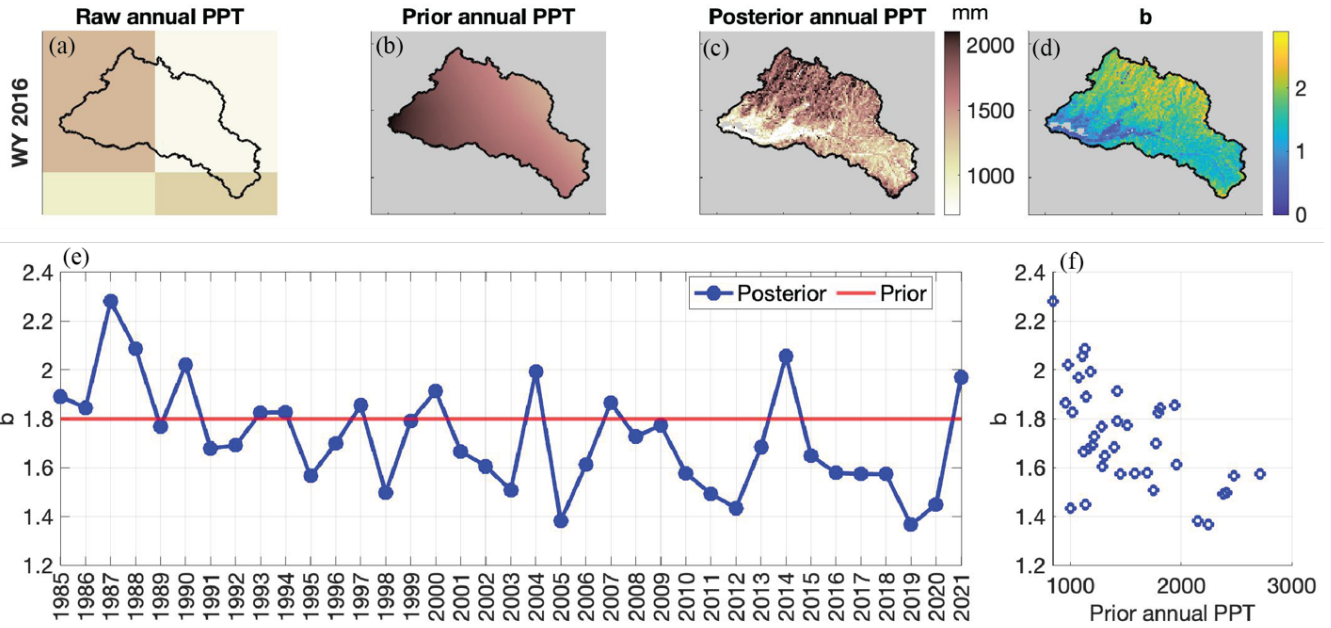
In addition to generating a high-resolution reference dataset of SWE estimates for a 37-year historical period to use

for validation, this application of the SWE reanalysis framework also yields a rich database of historical precipitation bias correction factors that are conditioned on assimilated fSCA measurements. These values provide insight into the historical distribution of precipitation bias and uncertainty (Fig. 3). Hereafter, and unless otherwise indicated, b will refer to the ensemble mean of the posterior b distribution; this is used interchangeably with “bias correction”. This database comprises 37 years *

100 ensemble realizations = 3,700 values of b at each pixel. A historical distribution of b can then be derived at each pixel and for each water year, as demonstrated in Liu and Margulis (2019). This study leverages the insights stored in b towards developing real-time SWE estimates by using them to inform the precipitation bias correction of real-time applications (section 2.4, Fig. 2). Note that the assimilation of fSCA constrains SWE, which mostly depends on snowfall. So while we are multiplying the total precipitation by b , we expect that any adjustments are primarily on snowfall. This implicitly assumes that

some of the factors leading to snowfall bias, such as orography, impact rain and snow similarly. This assumption is consistent with previous applications of this reanalysis methodology (e.g., Fang et al., 2022; Liu and Margulis, 2019).

Figure 3 illustrates how, for sample water year 2016, the b from the historical reference dataset provides valuable built-in downscaling and bias correction information. Note that the posterior precipitation has a much higher resolution than the raw MERRA2 input; for example, ridge and valley features are noticeable in Fig. 3c whereas the field is very coarse in Fig. 3a, and smooth and unresolved in the interpolated field of Fig. 3b. Furthermore, the raw MERRA2 input fails to capture the expected orographic effect whereas the posterior precipitation clearly shows more precipitation at higher elevations in the north and along the watershed ridgelines. The posterior b 's, which are informed by the pixel-wise fSCA ablation time series in the reanalysis (assimilation) step, are the multiplicative (bias correction) factors that bring out these features in the posterior precipitation. They contain both a spatially distributed pattern relating to topography and static physiographic features (Fig. 3d) as well as an interannual variation (Fig. 3e, f). The spatially distributed pattern effectively downscale the coarse-resolution input, and the interannual variation describes intensity-dependent yearly biases of the input (MERRA2 precipitation). We observe that, for the study domain, this interannual variation is correlated with the prior MERRA2 precipitation level: a higher watershed-average prior precipitation correlates with a lower watershed-average bias correction ($R = -0.6$) (Fig. 3f).



195 **Figure 3.** For sample WY 2016: (a) Raw MERRA2 annual precipitation at its original resolution. (b) Ensemble-mean annual prior precipitation, which uses the raw MERRA2 precipitation interpolated to the model resolution. (c) Ensemble-mean annual posterior precipitation. (d) Ensemble-mean of the posterior bias correction b . (e) Watershed-average ensemble-mean prior (red) and posterior (blue) b per the reference dataset over the period of record. (f) Scatter plot showing negative correlation between watershed-average annual prior precipitation and watershed-average posterior b . Note that for (c) and (d), a non-seasonal snow mask screens out model pixels located below 1,500 m, with less than 2 cm of climatological SWE, and/or categorized as glacier.

200

2.4 Design of real-time modelling and data assimilation experiments

We use the b database from the historical reference dataset to inform and develop value-added precipitation bias correction for the real-time experiments (Fig. 2). The list and characteristics of these experiments are tabulated in Table 1. Section 2.4.1 describes the bias correction approach for each experiment. Sections 2.4.2 and 2.4.3 provide further details about 205 the data assimilation experiments (fSCA and snow depth, respectively). Figure 4 provides an illustrative schematic of the precipitation bias correction, data assimilation, and resulting SWE estimation for a sample pixel (location A in Fig. 1a) and water year (WY 2017).

Note here that we are applying and evaluating these experiments in hindcast mode and are selecting 1 April as the target representative date. As such, we are testing these methods at the end of the accumulation season, when real-time SWE 210 estimates would provide the most value for water supply forecasts. We select 1 April because it has traditionally been used to approximate peak SWE in the Sierra Nevada and is when the key April-July water supply forecasts are made (e.g., He et al., 2016). For true real-time application in an operational context, other factors such as data latency and computation time should be considered.

Each experiment is evaluated by its ability to reproduce SWE spatial fields as compared to the historical reference 215 dataset on 1 April, and ASO-derived SWE on the validation day closest to 1 April. For both, we compute three metrics: Pearson

correlation coefficient R to quantify how closely the reference spatial distribution is captured, normalized root mean square difference (normalized by the observational mean, NRMSD, %) to measure bias and random error, and mean difference (MD, mm) to measure the average bias.

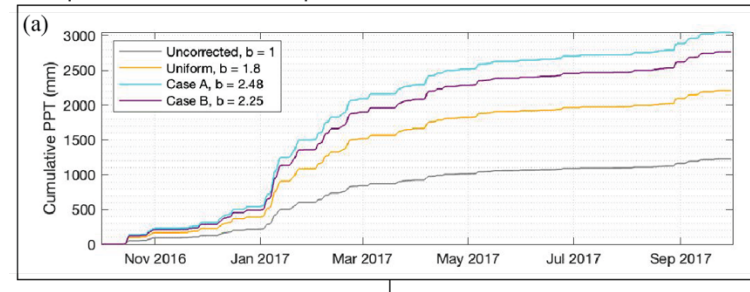
Note that the Uncorrected, Uniform, Case A and Case B experiments (Table 1) only use the forward-modelling component of the reanalysis framework; because there is no direct data assimilation in these experiments, there is no reanalysis step and therefore no posterior estimates. Instead, validation of these experiments is performed on the modelling-only prior estimates. The Case B + fSCA and Case B + SD experiments include data assimilation and thus yield posterior estimates.

Table 1. Summary of the methods applied to the six real-time experiments. The listed bias correction represents the mean of the prior b distribution. The “(x)” notation refers to the bias correction being a spatially distributed field, where x is each pixel in the watershed; b_{clim} refers to the climatological values over the entire period of record; b_{wet} refers to the average values from only wet years; b_{normal} from only normal years; and b_{dry} for only dry years.

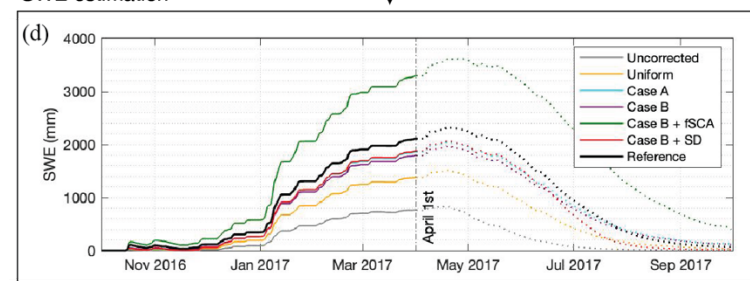
		Experiment name	Mean bias correction
Forward modelling experiments	Uncorrected		1
	Uniform		1.8
	Historically informed	Case A	$b_{clim}(x)$
Data assimilation experiments	Case B		$b_{wet}(x), b_{normal}(x), b_{dry}(x)$
	Case B + fSCA*		$b_{wet}(x), b_{normal}(x), b_{dry}(x)$
Case B + SD*			$b_{wet}(x), b_{normal}(x), b_{dry}(x)$

* In assimilation experiments, only observations up to 1 April are included.

Precipitation bias correction experiments



SWE estimation



Data assimilation experiments

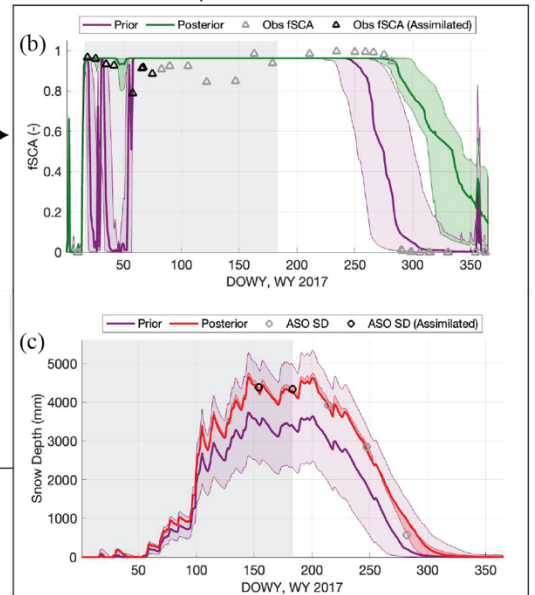


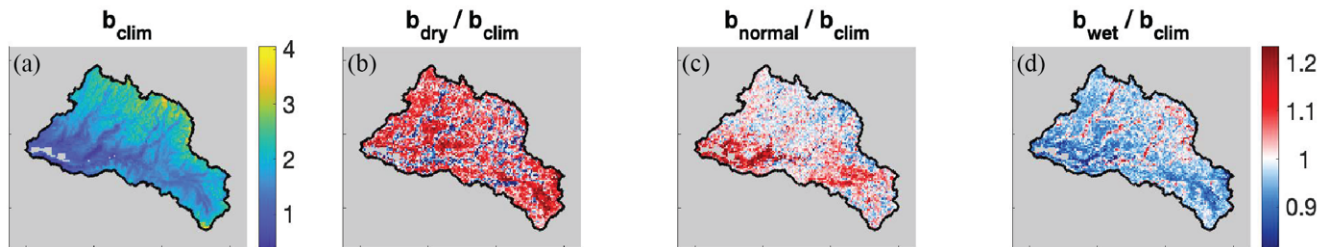
Figure 4. For a sample wet year (WY 2017) and sample pixel A: (a) Ensemble-mean cumulative prior precipitation for the four forward modelling experiments. (b) Example of how fSCA assimilation is applied. The prior is the Case B experiment, and the posterior the Case B + fSCA experiment. Note that both the median and interquartile range (IQR) for the prior and posterior ensembles are plotted. The assimilation window, indicated with a grey rectangle, ranges from the snow onset date to 1 April. Observations that fall within the assimilation window and on a day when the prior ensemble is non-zero are labelled “assimilated”. (c) Example of how snow depth assimilation is applied. Like (b), the prior is the Case B experiment, and the posterior is the Case B + SD experiment. The assimilation window ranges from the start of the water year to 1 April. (d) Ensemble-mean SWE time series

for the four forward modelling experiments, two data assimilation experiments, and the historical reference dataset. The outcome of these experiments is evaluated on 1 April.

2.4.1 Definition of precipitation bias correction factors

We generate a baseline, uninformed case where the prior precipitation is uncorrected (Uncorrected in Table 1, Fig. 240 4a). The Uniform experiment adjusts prior precipitation with a uniform (in time and space) mean prior b (Table 1) that matches that used in the historical reference dataset and defined in Fang et al. (2022). This represents the case for a simple precipitation bias correction. Note that we maintain the nominal CV and minimum/maximum values from Fang et al. (2022) for the prior b ensemble for this and all subsequent experiments; that is, we alter only the ensemble mean.

The more informed experiments leverage the database of historical b factors generated as a byproduct of the SWE 245 reanalysis framework. They vary from the less-informed cases (Uncorrected, Uniform) in two key ways: the prescribed precipitation bias corrections are spatially distributed, and historically informed. From the historical reference, we compute a spatially distributed climatological b for each water year, withholding the b value from a given year in deriving a long-term climatology for that year (Fig. 5a). These climatological values are used as the mean bias correction for the Case A experiment 250 (Table 1, Fig. 4a). Because we observe a relationship between precipitation level and watershed-average b in the historical reference (Fig. 3f), we also derive a bias correction that is conditioned on water year type. For each water year, we determine a type based on the historical prior precipitation (cumulative on 1 April), where $<30^{\text{th}}$ percentile is “dry”, $>70^{\text{th}}$ percentile is “wet”, and in between is “normal”. We take a spatially distributed average of the historical b ’s of all the other years classified in that water year type; that average becomes the mean value of bias correction for that year in the Case B experiment (Table 1, Fig. 5a). In this way, the bias correction applied in Case B differs by water year type, whereas in Case A it does not. In Fig. 255 5, we illustrate how the historical b factors across the watershed for wet years tends to be less than the climatological values (with the exception of headwater river valley bottoms, as shown in red in Fig. 5d); and those for dry years tend to be greater (Fig. 5b). In Fig. 4a, we see how the prior precipitation in Case B differs from Case A because of the difference in precipitation bias correction.



260 **Figure 5.** Per the historical reference: (a) climatological (WY 1985-2021) bias correction map. (b) The ratio between the dry year and climatological bias correction. (c) Same as (b) but for normal years. (d) Same, but for wet years.

The last two experiments include the assimilation of either fSCA or snow depth measurements; these experiments are subsequently referred to as Case B + fSCA and Case B + SD, respectively. The data assimilation methods are described further

in sections 2.4.2 and 2.4.3. We choose to use the Case B method of correcting prior precipitation for these experiments because

265 it represents the most informed and sophisticated bias correction.

2.4.2 Assimilation of fSCA observations

Previous data assimilation experiments that use fSCA to effectively improve SWE estimates have typically utilized measurements from both the accumulation and melt seasons (e.g., Girotto et al., 2014; Margulis et al., 2016; Fang et al., 2022), which are assimilated retrospectively in a single batch at the end of the water year. This is done with the understanding that it
270 is the fSCA ablation time series combined with estimates of snowmelt that is most directly connected to peak SWE. The value of fSCA measurements during the accumulation season is expected to be more limited because snow coverage is often complete or near-complete (i.e., fSCA = 1) when snow is accumulating in snow-dominated areas. Past studies have found limited to no improvement from prior modeled SWE estimates when assimilating fSCA observations over the accumulation season, independently from one another, or at sites which experience long periods of near-complete snow cover (Andreadis
275 and Lettenmaier, 2006; De Lannoy et al., 2010).

Here, we test whether there is any additional benefit in SWE estimation with bias-corrected precipitation when assimilating fSCA up to 1 April, and where in the watershed that benefit might be the greatest. We use the same methods described in section 2.3 to derive, screen, and assimilate fSCA observations, but only include the subset of fSCA observations that fall between a snow onset date and 1 April (Fig. 4b, more details about the assimilation window and the snow onset date
280 in Text S2). Note that not all pixels in the watershed assimilate the same number of fSCA observations for a given year because of differences in the snow onset date, cloud cover, and satellite orbital patterns. The average in the study domain over the period of record is about 7 usable observations per year but can vary between 0 to 24.

2.4.3 Assimilation of snow depth observations

The experiment with snow depth assimilation (Case B + SD) incorporates multitemporal lidar-derived snow depth
285 observations taken over the Tuolumne watershed by ASO (Painter et al., 2016) on and before 1 April. The observations cover the entire watershed (Fig. S3). In contrast to fSCA, snow depth observations are expected to provide more insight into accumulation season SWE because of the close relationship between snow depth and SWE. Margulis et al. (2019) demonstrated how the assimilation of even a single day of ASO snow depth observations was able to significantly improve posterior estimates of SWE later in the year. Here, we seek to quantify how much assimilating snow depth observations could improve upon SWE
290 estimates that already incorporate a historically informed precipitation bias correction. We use data for three representative years: WY 2015 (dry), 2016 (near average), and 2017 (wet). The number and dates of the ASO observations used for assimilation and validation purposes are summarized in Table 2. Prior to assimilation, the 50 m ASO snow depth product was regridded to the modelling resolution. Following Margulis et al. (2019), we specify a measurement error standard deviation of 5 cm. Figure 4c illustrates snow depth assimilation for a sample model pixel: the observations on March 3rd and 1 April of this
295 year fall within the prior ensemble, and so are assimilated and yield a higher posterior mean and narrower ensemble.

300 **Table 2. ASO acquisition DOWY (day of water year) and their corresponding dates. The dates of the observations used for assimilation and for validation (i.e., the day closest to 1 April) are indicated for each WY.**

		Assimilated	Validation
WY	2015	140 (Feb 17), 156 (Mar 5), 176 (Mar 25)	185 (Apr 3)
	2016	178 (Mar 26), 184 (Apr 1)	190 (Apr 7)
	2017	154 (Mar 3), 183 (Apr 1)	214 (May 2)

2.5 Connection to streamflow

We further evaluate the real-time SWE experiments by their ability to yield snowmelt estimates and streamflow forecasts that match observed streamflow at the TGC (Tuolumne River at the Grand Canyon) USGS gauge. Note that for this comparison, the focus is on a subwatershed that drains through the TGC gauge (Fig. 1a). Continuous daily streamflow records 305 are generated from observations at the gauge for WYs 2009-2021 (Text S3).

We measure how well daily watershed-average snowmelt estimates correlate with daily observed streamflow for the key forecasting period April-July with Pearson correlation coefficient R. For each experiment, the SWE reanalysis framework is run forward in time from 1 April with the known meteorological forcings of that year, yielding “perfect” hindcasts for SWE and snowmelt. Snowmelt is estimated as the negative daily changes in SWE, assuming sublimation is negligible.

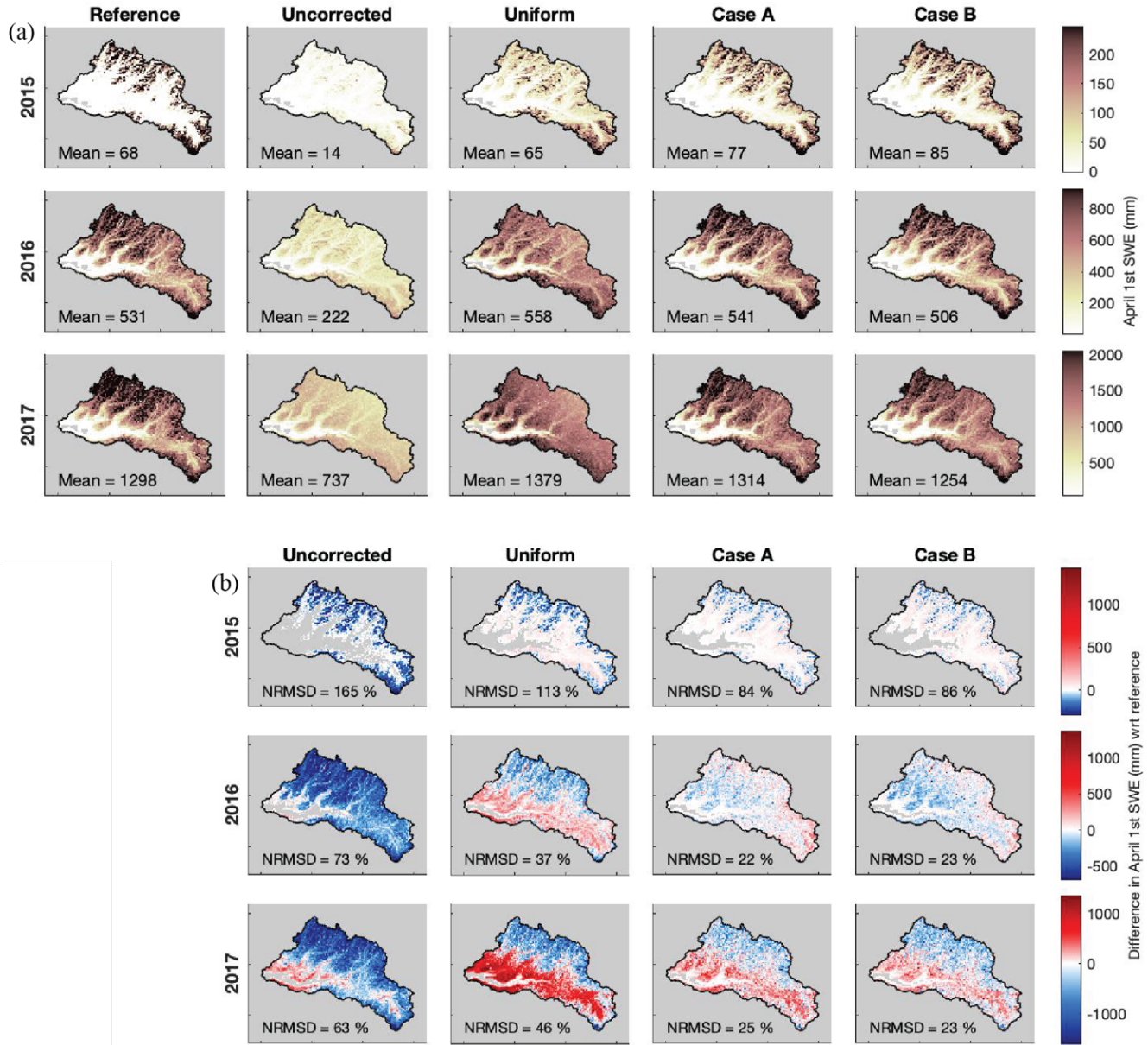
310 We quantify the ability of watershed-average estimated 1 April SWE to predict April-July (AJ) streamflow volume with a historical linear regression. For a given year, we build a regression from all other years (i.e., excluding the one being evaluated) using observed AJ streamflow as the predictand (Fig. S8). Observed AJ streamflow from WY 2019 is excluded because of incomplete observations (Fig. S2). We quantify the bias and mean absolute differences between the predicted 315 volumes from the experiments and the reference. Because we are treating the historical reference dataset as the ground truth in this study, the predicted volume from its SWE estimates is treated as the “best case” prediction and so is the target in this comparison. The relationship between estimated 1 April SWE and observed streamflow is affected by other factors like rainfall and soil moisture conditions, which make errors between the predicted and observed streamflow volume inevitable and not the focus of the study. Note that for this analysis, the snow depth experiment is excluded because it only has 3 years of results.

3 Results and Discussion

320 3.1 Value added from historically informed precipitation bias correction

Maps of 1 April SWE estimates and their difference relative to the historical reference (Fig. 6) highlight key differences across experiments; in particular, these show how using a historically informed precipitation bias correction (Case A and Case B) yields 1 April SWE that better matches the reference. Here, the reference is the posterior SWE estimates from

the historical reference dataset which is constrained by the full set of fSCA observations across the water year. Notably, we
325 can see how Case A and Case B produce 1 April SWE distributions that are much better spatially-resolved than the less-informed Uncorrected and Uniform experiments: individual ridges and valleys are more prominent and match the historical reference more closely (Fig. 6a). This is also notable in the maps illustrating bias in SWE: in the Uniform experiment, a strong geographical pattern exists in WY 2016 and 2017, where the lower-elevation areas of the watershed (generally, the southern half) consistently show a positive bias in SWE estimation, and the higher elevations show a negative bias (Fig. 6b). This
330 geographical distinction is lessened in Case A and Case B in 2015 and 2016, and greatly reduced in 2017. This illustrates that the historically informed spatially distributed bias correction is able to correct biases in input precipitation that are related to elevation and topography, whereas the uniform bias correction smooths over these spatial differences. Effectively, the spatially distributed bias correction downscale coarse-resolution input. We also see that Case A and Case B yield relatively similar results in terms of the spatial distributions and magnitudes of error.



335

Figure 6. (a) Maps of 1 April SWE for the historical reference, Uncorrected baseline, and three experiments for three representative water years: 2015 (dry), 2016 (normal), and 2017 (wet). (b) Maps of the difference in 1 April SWE (experiment - reference) for the same years and experiments. The NRMSD relative to the reference is included. Pixels where both the reference and experiment estimate 0 SWE are greyed out in addition to the mask in these maps.

340

All modelling-only experiments (Uniform, Case A, Case B) outperform the Uncorrected baseline in at least two 1 April SWE metrics (Fig. 7e-g). The greatest reduction in error relative to the Uncorrected baseline occurs when a spatially distributed bias correction is used: on average across all years in the record, Case A and Case B reduce NRMSD by 58% (to

33%), improve R by 43% (to 0.9), and reduce bias (MD) by 88% (to -41 mm) and 85% (to -52 mm), respectively (Fig. 7e-g).

The limited difference in performance between the two cases suggests that the primary value of the historical database of bias
345 correction distribution lies in its description of the (more or less static) spatial distribution of precipitation bias, rather than its temporal patterns or uncertainty. That is, the historically-informed bias correction is very effective at downscaling coarse-resolution input (as is done in Case A), but less effective at describing interannual bias (as is additionally done in Case B). A more simple uniform bias correction is also effective at reducing error but to a lesser degree: the Uniform case reduces average NRMSD by 35% (to 51%) and MD by 97% (to -11 mm), and yields an insignificant average impact on R (Fig. 7e-g). Note
350 that the MD metric averages values across the watershed and so does not represent the spatial spread of error in these estimates (Fig. 6b). For the Uniform experiment in particular, a lower watershed-average MD masks high positive and negative errors across the watershed (Fig. 6b).

The performance of these experiments varies by year. For example, in WY 2015, which was historically dry in the Hetch Hetchy watershed, NRMSD is the highest across all experiments (Fig. 7b). Although the two spatially distributed
355 precipitation bias corrections yield similar results in most cases, Case B (where the bias correction is also differentiated by water year type) has an 8-30% lower bias than Case A in low and normal snow years (Fig. 7g). This indicates that differentiating the bias correction by water year type further reduces bias in years with lower snow accumulation. In those years, the bias correction is generally higher than the climatological mean (Fig. 5b), which, when applied to prior precipitation, effectively increases the snowfall input and reduces the negative SWE bias. On the other hand, Case B has a more negative SWE bias in
360 high snow years than Case A (Fig. 7g); in these high snow years, the bias correction is generally lower than the climatological value and so when applied to prior precipitation would reduce input snowfall. The impact of a uniform bias correction factor also varies slightly by water year type: Uniform improves R from the Uncorrected baseline in low snow years, but reduces R in normal or high snow years, indicating a poorer spatial correlation to the reference in years with higher snow accumulation (Fig. 7f). High snow years in Uniform are also the only years to show an average positive bias (Fig. 7g), suggesting the uniform
365 bias correction generates higher input precipitation than the reference dataset in higher snow years. This is consistent with the observation in Fig. 3f that, historically, wetter years correlate with a lower watershed-average bias correction; in these years, the posterior bias correction is less than the uniform value.

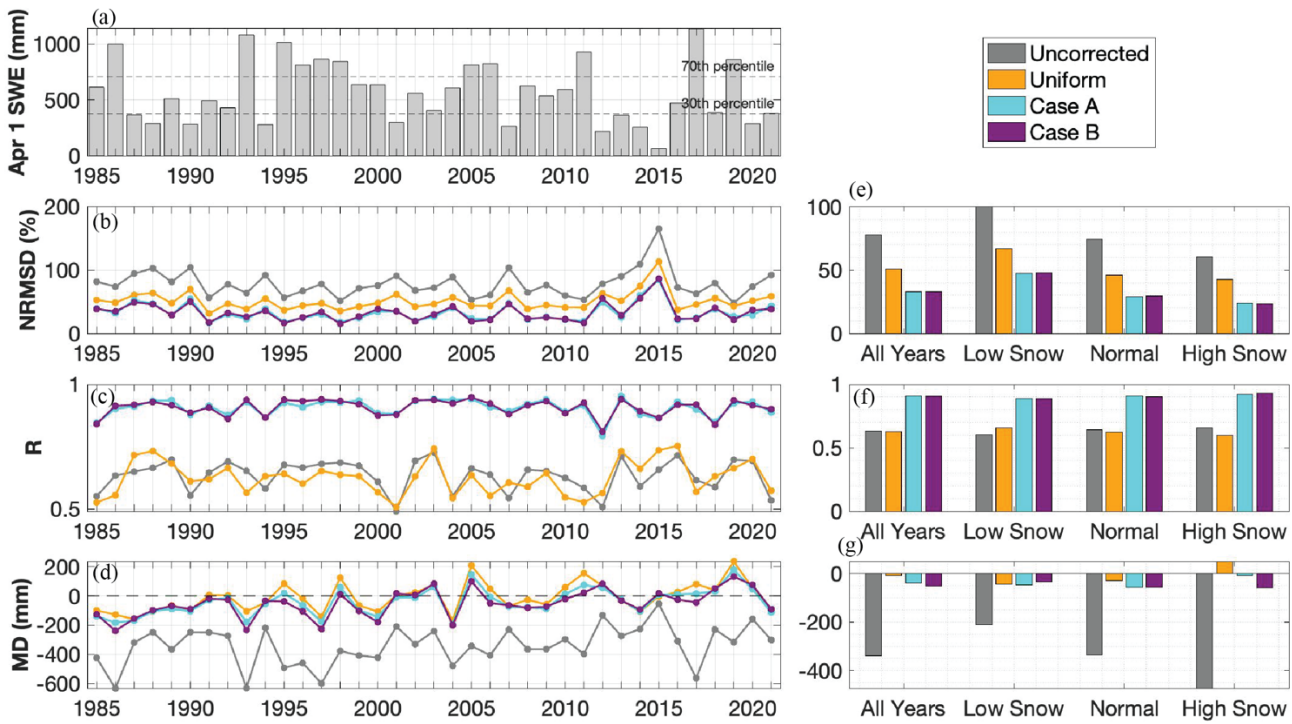


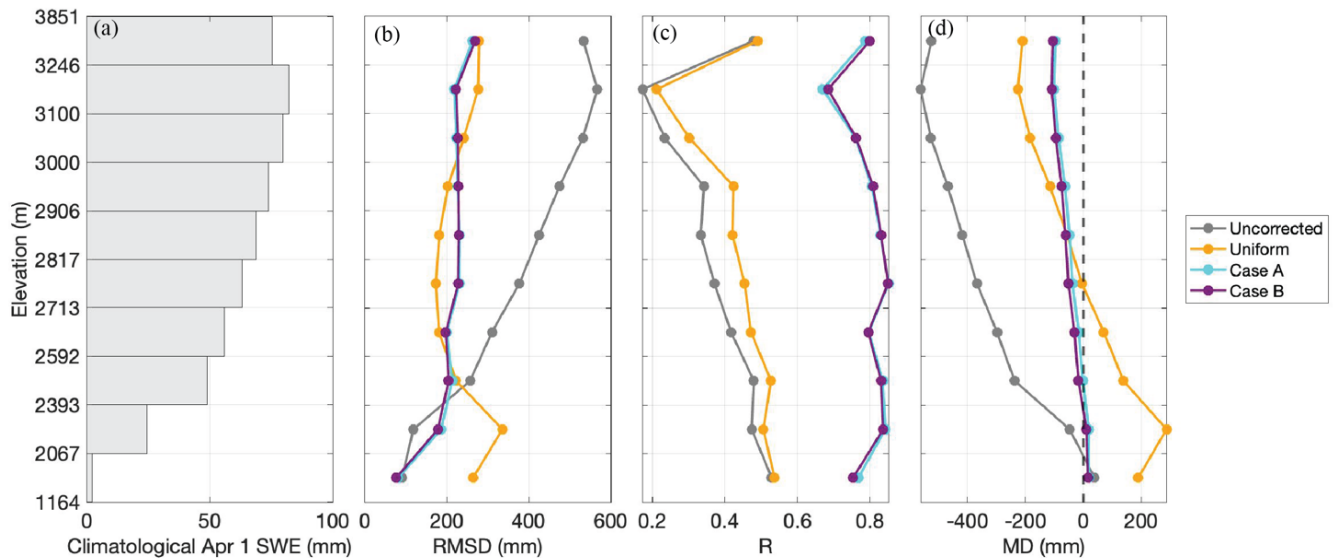
Figure 7. (a) Watershed-average 1 April SWE per the historical reference dataset. The 30th and 70th percentile are indicated with horizontal lines, and differentiate between low snow (below 30th percentile), normal snow, and high snow (above 70th percentile) years. (b-d) Yearly performance metrics (NRMSE, R, MD; top to bottom) for 1 April SWE in the four modelling-only experiments as compared to the reference. (e-g) Performance metrics (NRMSE, R, MD; top to bottom) averaged across all years, low snow years, normal snow years, and high snow years.

370

Figure 8 illustrates the distribution of error in SWE in these experiments across elevation bands. At low elevations (below 2600 m), the Uncorrected baseline tends to have the least error (lowest RMSD), but also a significant negative bias (MD) that persists across all elevations and indicates an underestimation of SWE (Fig. 8b, d). The other three experiments, which incorporate varying levels of precipitation bias correction, instead overestimate SWE at low elevations: Case A and Case B by small magnitudes (~5-10 mm) and Uniform by a greater magnitude (~200 mm) (Fig. 8d). Spatial distribution of SWE is best represented by Case A (with Case B a close second) at low elevations, as indicated by the highest R (Fig. 8c). At mid elevations (between 2600 m and 3000 m), the lowest error (RMSD) occurs in the Uniform experiment, then Case B and Case A, and then Uncorrected (Fig. 8b). The bias in Case A and Case B is consistently negative at mid elevations, with Case A having the slightly lower magnitudes (Fig. 8d). The bias in the Uniform experiment switches from positive to negative at around 2760 m (Fig. 8d); this trend demonstrates cancellation effects happening in the watershed-averaged bias, where the watershed-average value in Fig. 7 may be low despite both high positive and negative biases at different elevations. Error across all three performance metrics increases more steadily and more steeply with increasing elevation in the Uncorrected baseline than the Case A or Case B experiments (Fig. 8b-d). This implies that the spatially distributed precipitation bias correction applied to the latter two is effective at reducing error across the watershed, especially at higher elevations where

most SWE is located. At high elevations (above 3000 m), the lowest error (RMSD) and bias (MD) occurs in Case A, with Case B as a close second and Uncorrected as significantly worse (Fig. 8b, d). The spatial distribution of SWE (R) is best portrayed by Case B, with Case A close behind (Fig. 8c). Notably, the elevation band (3100-3246 m) with the lowest R across all experiments is also the one with the highest climatological April 1 SWE (Fig. 8a, c). This suggests that this elevation band could benefit from ablation season and post-ablation fSCA assimilation, which is included in the historical reference. All experiments underestimate SWE at high elevations (Fig. 8d), indicating that the spatially distributed precipitation bias corrections are not enough to fully compensate for the negative bias in SWE estimation at high elevations, although it does reduce that bias.

Overall, including a spatially distributed precipitation bias correction significantly improves spatial SWE estimates across all elevation bands, as indicated by consistently higher R values in Case A and Case B than both the Uncorrected and Uniform experiments (Fig. 8c). This bias correction also yields error that is more uniform across elevation bands; crucially, it reduces error more significantly at higher elevations where more SWE accumulates (Fig. 8b, d). It is worth noting that, to the extent that reanalysis precipitation products such as the MERRA2 input used in these experiments get informed by existing in situ precipitation gages, those data are generally at lower elevations. This emphasizes the need to get accurate spatially distributed bias corrections that adjust uncertain precipitation inputs at higher elevations where most SWE accumulates.



405 **Figure 8.** (a) Long-term (WYs 1985-2021) average 1 April SWE in each of 10 elevation bands of the watershed. Elevation band bounds were determined by distributing an even number of model pixels into each band. (b-d) Long-term average RMSD, R, and MD (left to right) for each elevation band for the Uncorrected baseline and three modelling-only experiments.

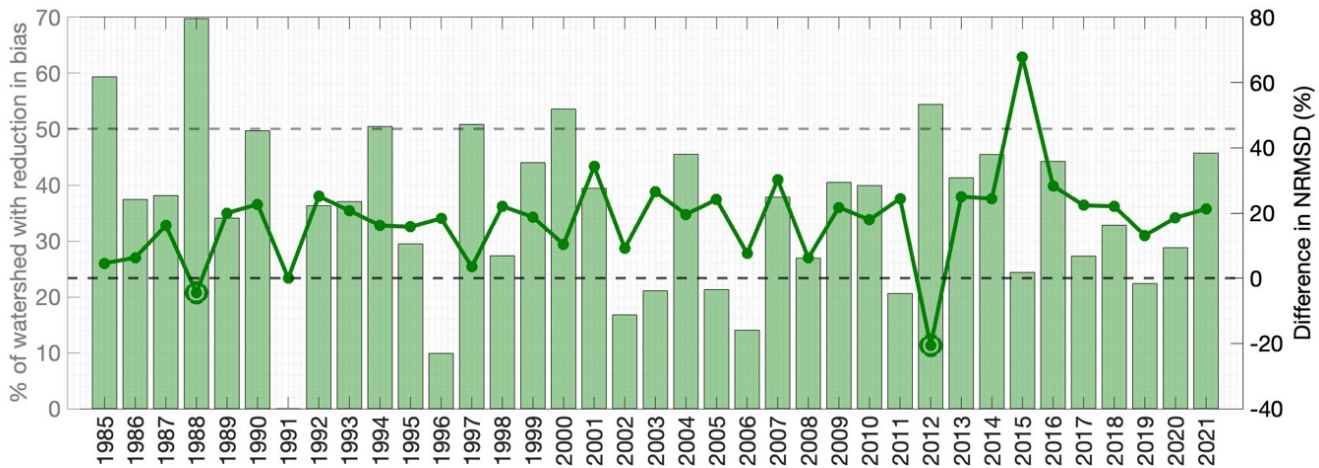
3.2 Additional value through data assimilation

3.2.1 fSCA assimilation

The value of assimilating fSCA to estimate SWE lies primarily in its ability to track the loss of snow cover during the melt season, so the expectation for additional insight from assimilating fSCA observations only before 1 April (as was done in the Case B + fSCA experiment) is low. This is confirmed by the results: when looking at the overall impact of fSCA assimilation on 1 April SWE estimates, the watershed-scale NRSMD is reduced from the prior in only 2 of 37 years (Fig. 9). A further 7 years show a posterior NRMSD within only 10% of the prior, indicating limited difference. In the remaining years (the majority), fSCA assimilation brings the posterior estimates further from the historical reference and increases the NRMSD (Fig. 9). Note that here, the experiment uses the spatially distributed precipitation bias correction from Case B. This implies that accumulation season fSCA observations, which comprise most of the observations before 1 April, are more noisy than helpful in data assimilation. In fact, assimilating these observations is detrimental to overall SWE accuracy in most years (Fig. 9). Overall, this method is not a useful approach to improving real-time 1 April SWE, especially when the precipitation input is already bias-corrected as is the case here.

We find that the timing of fSCA observations in the water year is significant to determining whether their assimilation reduces error in SWE estimates. For example, in WY 1988, only 1-2 fSCA observations were assimilated into the fSCA experiment, but all of these occurred after pixel-wise peak SWE and before 1 April (Fig. S4a). In that year, 70% of pixels showed a reduction in posterior error relative to the reference, and the watershed-scale NRMSD was reduced 5% (Fig. 9). In WY 2012, pixel-wise peak SWE averaged after 1 April for the watershed, but the NRMSD was still reduced (by 21%) with fSCA assimilation because enough fSCA observations (6-10) were assimilated at low-elevation pixels (Fig. S4b). Note that in cases with fewer fSCA observations during the accumulation season, there is often degradation in the posterior SWE estimate.

Individual pixels in the watershed can show improvement with fSCA assimilation even when the total error is increased. The absolute bias relative to the reference is reduced at over 50% of the pixels in the watershed with fSCA assimilation in 7 years (Fig. 9). The pixels where fSCA assimilation reduces error tend to have an earlier peak SWE, lower elevation, and higher number of fSCA observations assimilated (Fig. S5). In most years, there is a statistically significant difference in all these variables between the pixels with an improvement and those without an improvement. This is consistent with the finding in Andreadis and Lettenmaier (2006) that improvements in SWE estimation from fSCA assimilation are more evident at lower elevations and during snowmelt.



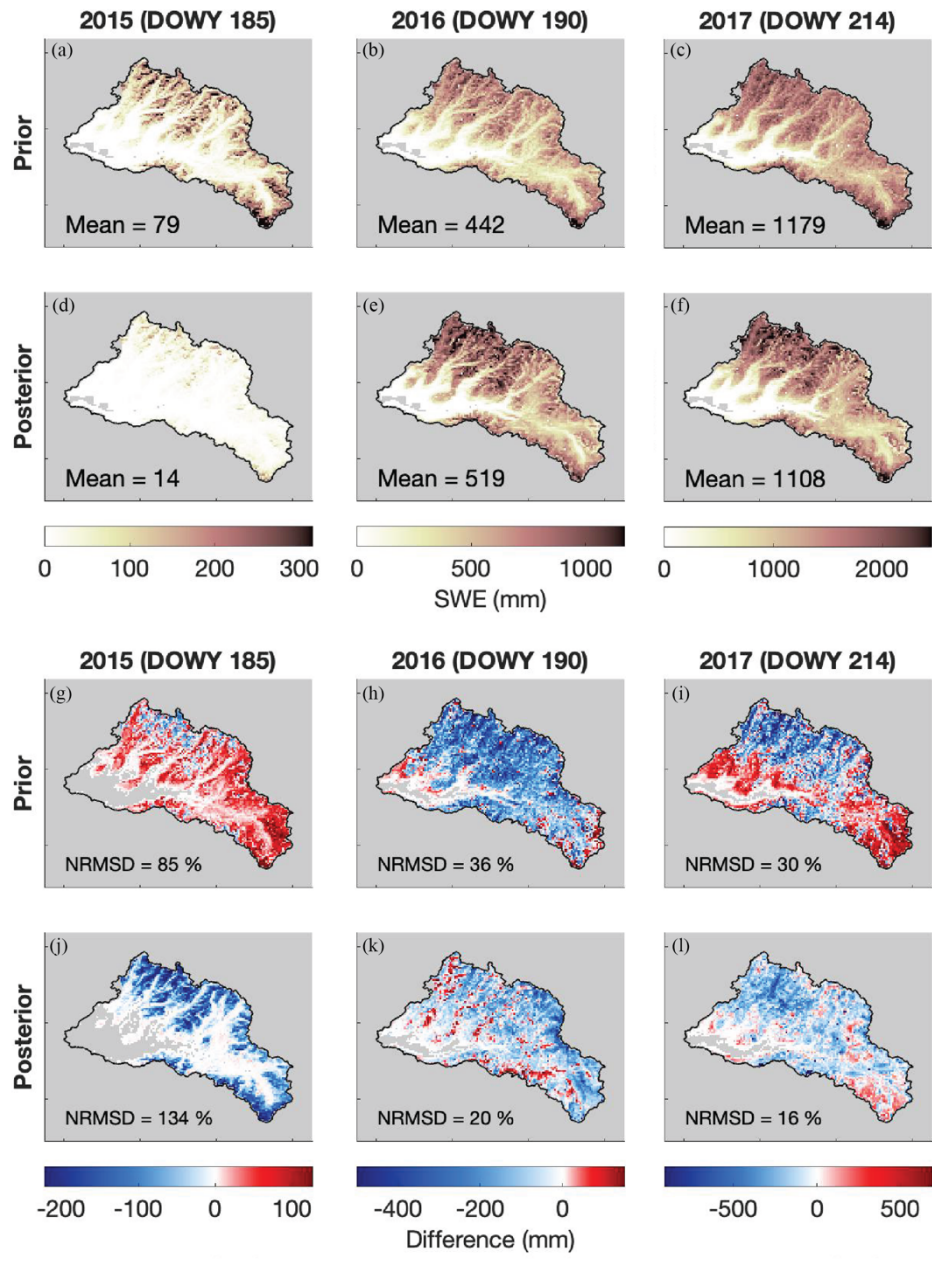
435 **Figure 9.** The height of the bar indicates the percent of pixels that show a reduction in error (absolute difference) relative to the
 440 reference when fSCA assimilation is applied for that WY (left axis). The solid line indicates the differences in watershed-scale
 NRMSD relative to the reference between the prior and posterior estimates (i.e., $\text{NRMSD}_{\text{post}} - \text{NRMSD}_{\text{prior}}$) (right axis). The plot
 points below 0 are highlighted with an extra circle; in these years, the posterior estimate yields a lower NRMSD than the prior. The
 grey dashed line indicates the point at which 50% of the watershed shows a reduction in bias (left axis); the black dashed line
 indicates where the posterior NRMSD is less than the prior (right axis). Note that in 1991, no fSCA observations were assimilated
 so there was no change from the prior to the posterior SWE estimates.

3.2.2 Snow depth assimilation

445 In addition to mostly reducing watershed-scale average error (as expected), snow depth assimilation brings more
 spatial heterogeneity to SWE estimates and reduces pixel-wise bias. Note that for this comparison, the reference is SWE from
 450 the ASO observations succeeding the last one that was assimilated; that is, day of water year (DOWY) 185 in WY 2015, 190
 in 2016, and 214 in 2017. In the maps of Fig. 10, we observe that in WY 2016 and 2017, the posterior estimates show a wider
 range in SWE than the prior, with higher SWE estimates at higher elevation pixels. Note that this prior-posterior pair uses the
 historically informed spatially distributed bias correction from Case B. In WY 2015, we observe how most of the watershed
 has already lost its snow cover by the day of comparison according to the posterior estimates (Fig. 10a), which contributes to
 the poor performance of snow depth assimilation in this year.

455 In both WY 2016 and 2017, we observe a decrease in pixel-wise error with snow depth assimilation. In 2016, most
 of the watershed demonstrates an underestimation of reference (ASO) SWE in the prior; this is lessened in the posterior, with
 some valleys showing slight overestimation (Fig. 10h, k). In 2017, the prior shows an underestimation of ASO SWE in the
 northern high-elevation region of the watershed and an overestimation in the southeastern headwaters and low river valley
 area, some of where ASO observes no snow by this time. In the posterior, the magnitude of pixel-wise error is universally
 decreased, more of the watershed underestimates ASO SWE, and the lack of snow in the low river valley areas is more correctly
 captured (Fig. 10i, l). In the prior in 2015, most of the watershed except for higher elevation ridge areas in the north shows an
 overestimation of the reference SWE, including areas where ASO observes no snow cover (Fig. 10g). The posterior SWE map
 shows an almost universal underestimation of observed ASO SWE in this year, except for the areas where the estimates

460 correctly predict no snow cover (Fig. 10j). This is consistent with the higher watershed-scale errors observed in the estimations with snow depth assimilation on the validation day in 2015 from Fig. 11.



465 Figure 10. (a-c) Maps of prior SWE for the Case B + SD experiment on the validation day in three water years. (d-f) Maps of posterior SWE for the Case B + SD experiment. (g-i) Maps of the difference between prior SWE and ASO-derived SWE. (j-l) Maps of the difference between the posterior SWE and ASO-derived SWE. Values of NRMSD relative to the ASO-derived SWE are listed. Pixels where both the experiment and the ASO-derived SWE have 0 SWE are greyed out in addition to the mask.

Figure 12b demonstrates how, for a sample model pixel, the two ASO snow depth observations assimilated in 2016 can bring the prior estimate up to a posterior that better fits the observations both before and after 1 April. In both WYs 2016 and 2017, the Case B + SD experiment shows the lowest NRMSD (81% less than the Uncorrected baseline) and the highest R (Fig. 11a, b). This also holds true for bias (MD) in WY 2016 (Fig. 11c). In all three years, Case B + SD shows a negative bias, indicating that posterior SWE estimates are consistently underestimated (Fig. 11c). Assimilating snow depth observations reduces the prior NRMSD by 43-46% and increases the R by 6-12% in WYs 2016 and 2017 (Fig. 11a). Note that for the Case B + SD experiment, Case B represents its prior (i.e., before assimilation).

In WY 2015, the outcome of the Case B + SD experiment is different on its validation day. On the days when ASO data is assimilated, the posterior SWE estimates successfully (and as expected) reduce error metrics from the prior (Fig. S6) but by the validation day on DOWY 185, 42% of the basin (mostly higher-elevation higher-snow areas, Fig. S7) has a greater bias in posterior SWE than in the prior. Although overall error is still reduced from the Uncorrected baseline on this day, NRMSD and MD are greater, and R is less, in the posterior than in the prior (Fig. 11). We hypothesize that anomalies in precipitation input that occur after assimilation explains the poor performance of snow depth assimilation on this day (Fig. 12a). Of the pixels in the watershed that exhibit higher error in the posterior than the prior estimates, 96% experienced an increase in observed snow depth from DOWY 176 (the last day when observations are assimilated) to DOWY 185 (the validation day) (for example, Fig. 12a). Note that, in most cases, this increase in observed snow depth corresponds to a decrease in observed SWE (Fig. 12b); this implies a decrease in ASO-derived snow density, which is consistent with a fresh snowfall event. The precipitation forcing around those days however does not reflect a snowfall event. This inconsistency between precipitation forcing and observations, and the fact that it happened after the last assimilated observation and that WY 2015 was an exceptionally dry year, explains the negative bias at those pixels and in the watershed by the validation day in 2015.

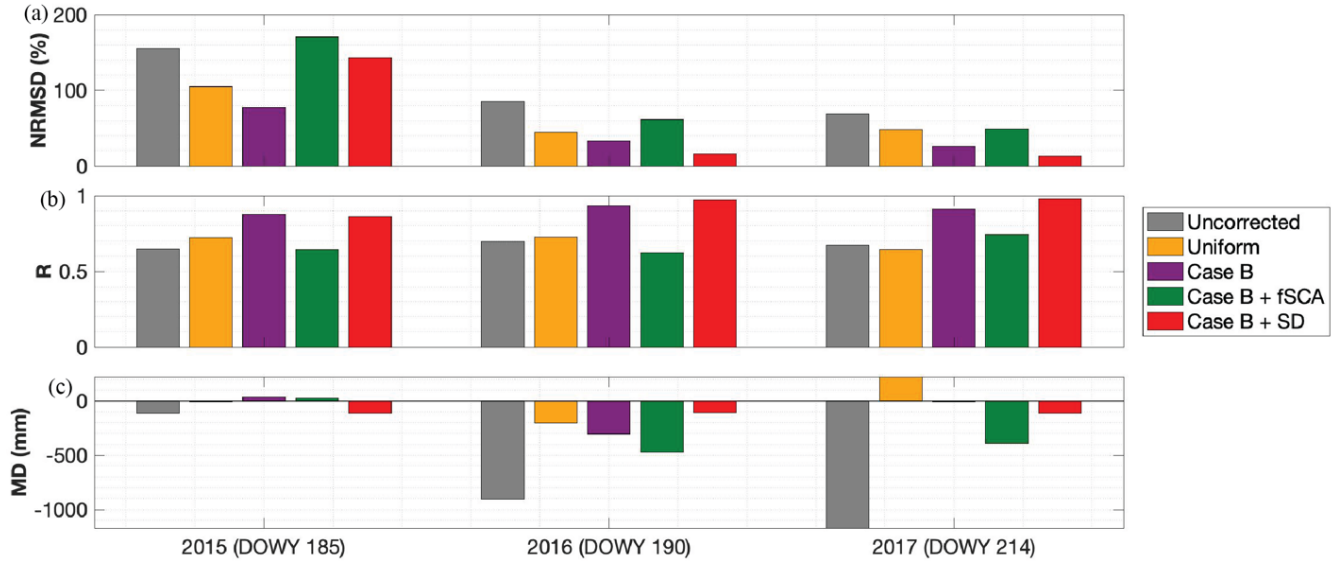


Figure 11. Summary of performance metrics: (a) NRMSD, (b) R, (c) MD, relative to ASO-derived SWE on the validation day for WY 2015, 2016, and 2017. Because of the similarities between Case A and Case B, only Case B metrics are included here.

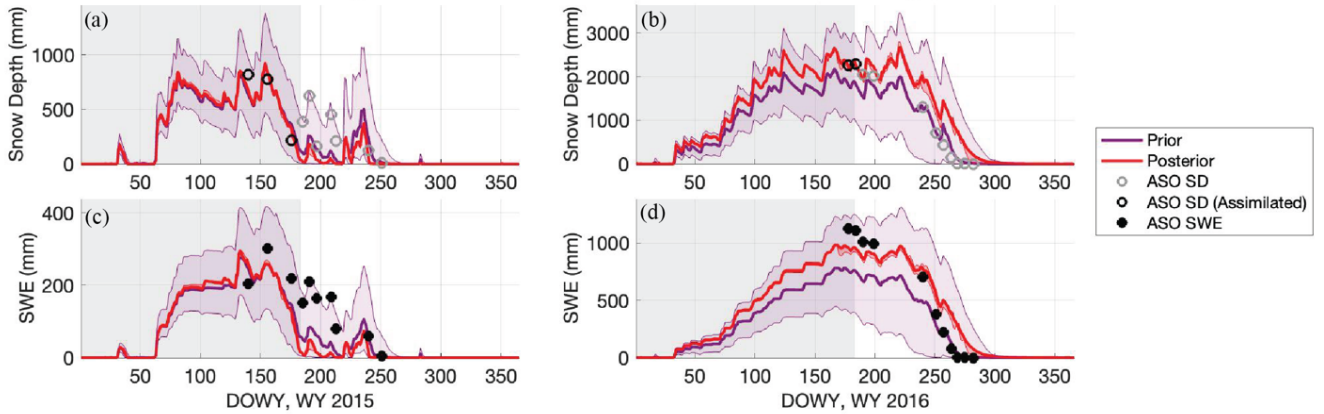


Figure 12. Sample time series illustrating snow depth assimilation at a sample model pixel in (a) WY 2015 and (b) WY 2016. The prior ensemble is in purple; the posterior in red. Note that both the median and interquartile range (IQR) for the prior and posterior ensembles are plotted. The assimilation window is indicated with a grey background rectangle. The bottom two plots illustrate prior and posterior ensemble mean and IQR for SWE estimates in (c) WY 2015 and (d) WY 2016.

495 3.3 Value for streamflow forecasting

A key purpose of 1 April SWE estimates is to support streamflow forecasts for spring and summer water supply. We argue that snowmelt is a reasonable proxy for streamflow in this case because Hetch Hetchy is a snow-dominated watershed. We observe that all experiments using bias-corrected precipitation are effective at yielding post-1 April snowmelt estimates

that correlate better to observed streamflow than the Uncorrected baseline. Fig. 13a-c illustrates the daily time series of
500 simulated snowmelt and observed streamflow for April-July in WYs 2015-2017. We observe that the daily simulated snowmelt reasonably captures peaks in observed streamflow: for example, the peak at the end of June 2017 which presumably is driven by a large snowmelt event (Fig. 13c). Some snowmelt is expected to infiltrate into the soil column, store in high alpine lakes, or evaporate before reaching the river during the April-July time period.

We acknowledge this discrepancy between snowmelt and streamflow magnitudes by quantifying the correspondence
505 of snowmelt to streamflow with a correlation coefficient (R); for a more thorough comparison, a hydrologic model is recommended to explicitly track downstream storage and fluxes that the snow model alone does not. We test different lag times between snowmelt and streamflow and find the highest correlations with 1 day lag. We find that these correlations are significant and higher than that for the Uncorrected baseline in every year for every bias-corrected experiment (except for Case B + SD in 2015); on average, by 31-39% (Fig. 13g, h). In WY 2016, the highest correlation occurs in the experiment with
510 snow depth assimilation (Fig. 13g). Excluding this experiment because it only yields results for a subset of WYs, the highest average annual correlation coefficient (0.74) is shared amongst Case B and Uniform. It is worth noting that Uniform has cancellation of errors at the watershed scale; that is, high and low within-watershed biases in 1 April SWE are averaged out (as demonstrated in Fig. 6b). Here, by aggregating snowmelt to watershed-average values, we are likely similarly averaging out within-watershed biases. The experiment with accumulation season fSCA assimilation consistently has lower correlations
515 than those without in all water year types (Fig. 13h). This is consistent with the result that the Case B + fSCA experiment often yields higher errors in 1 April SWE (Fig. 9). In low snow years, the highest correlation occurs with Case B snowmelt; in high snow and normal years, the highest correlation is with Uniform (Fig. 13h).

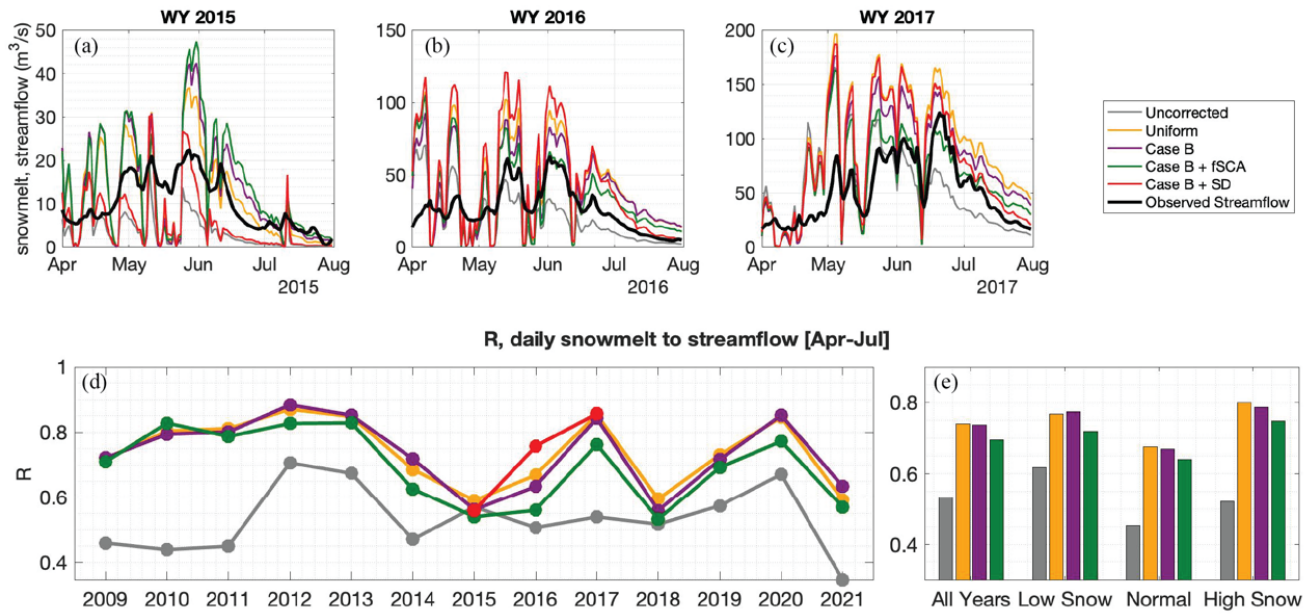


Figure 13. (a-c). Daily snowmelt for the Uncorrected baseline and four experiments, and observed streamflow for April-July in WYs 520 2015, 2016, 2017. Note that because Case A and Case B had similar results, only Case B is included here. (d) Correlation R (lag-1) 2015 between daily estimated snowmelt and observed streamflow for WYs 2009-2021. (e) Average correlation for all years, low snow 2016 years, normal years, and high snow years. Note that these averages exclude the Case B + SD experiment because it only includes 3 2017 years of estimates.

Figure 14 summarizes results from a linear regression model which predicts April-July (AJ) streamflow volume from 525 watershed-average 1 April estimated SWE. The experiment with snow depth assimilation is excluded because it only has 3 years of estimates. The multi-year average adjusted R^2 for these regression models, developed and applied separately for each 530 experiment-year, range between 0.94 and 0.96 (illustrated in Fig. S8); these high values emphasize the strong relationship between 1 April SWE and AJ streamflow. In Fig. 14, we compare the predicted streamflow volume from the experiments to the predicted streamflow volume from the historical reference. The predicted AJ streamflow from reference 1 April SWE estimates is considered the “best case” prediction and so is the target in this comparison.

The yearly differences between the experiment and reference AJ streamflow volume range between -30% and 70% (Fig. 14a). The highest differences occur in 2015; this is a historically dry year which also exhibited high errors in 1 April SWE estimates (Fig. 7). Because these yearly differences might cancel each other out in a multi-year average, we also look at the mean absolute differences (MAD) across water year types to gauge the magnitude of error (Fig. 14c). Generally, the bias 535 and MAD in low snow years is the largest and positive, signifying an overestimation of the reference AJ streamflow volume. The MAD in normal and high snow years are similar in magnitude, but the bias is opposite in direction (positive in high snow and negative in normal) and less in normal years. Overall, the average bias and MAD is reduced from the Uncorrected by the bias-corrected experiments across all water year types (except for Case B + fSCA in high snow years MAD) (Fig. 14a). The greatest improvement in streamflow prediction from the Uncorrected occurs with the Case B 1 April SWE estimates, which

540 reduces average bias by 52% and MAD by 26%. The Uniform experiment is a close second (46% and 25% less average bias and MAD). This is consistent with the error reductions in 1 April SWE observed when using bias-corrected precipitation (Fig. 7). It is worth noting that averaging over the watershed, as is done to obtain the 1 April SWE predictor for AJ streamflow, could mask spatially distributed error (which is high in the Uniform experiment, Fig. 6b). A spatially distributed land surface model would provide the opportunity to further evaluate how improvements in the spatial distribution of SWE, as is observed 545 to happen with spatially distributed historically informed precipitation bias corrections (Fig. 7, Fig. 8), affects runoff modelling and streamflow forecasts.

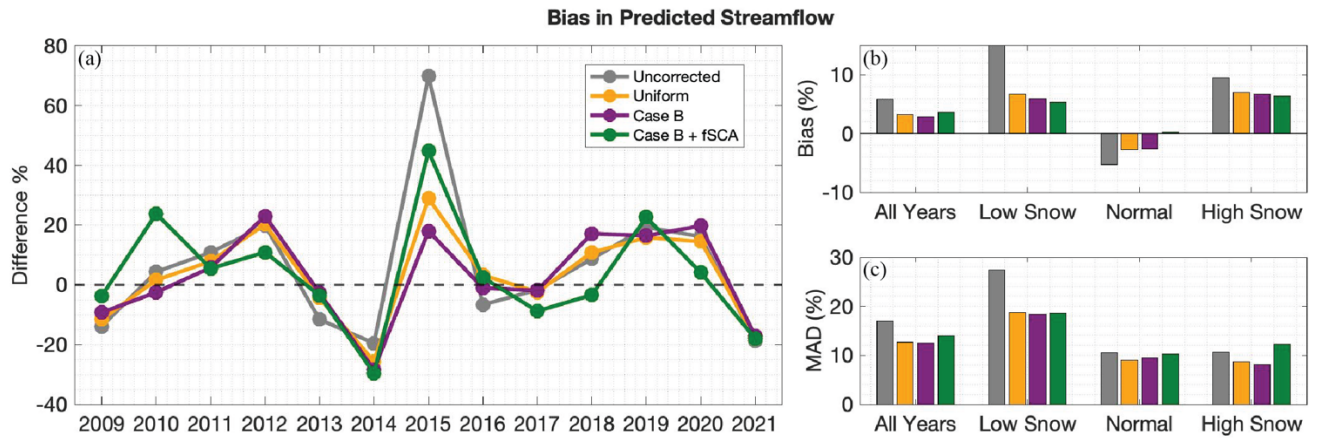


Figure 14. (a) Difference (%) computed between the predicted April-July streamflow volume of the experiments and the historical reference. (b) Average biases for all years, low snow years, normal years, and high snow years. (c). Mean absolute differences (MAD).

550 4. Conclusions

Results demonstrate that spatially distributed historically informed precipitation bias correction significantly enhances SWE estimates. With respect to 1 April SWE fields, it reduces error (NRMSD) by 57-58%, increases spatial correlation (R) by 43%, and decreases bias (MD) by 85-88%. A simpler, spatially uniform bias correction (as used as a first 555 guess prior in the original reanalysis methodology) also reduces error relative to uncorrected precipitation but to a lesser degree.

We find that the spatially distributed historically informed bias correction yields SWE error that is not only lower but more 560 homogeneous across elevation bands than the uniform bias correction; crucially, this means error is reduced more significantly at higher elevations where SWE accumulation is greater. It also significantly improves SWE spatial estimates as indicated by higher R values across all elevation bands. As illustrated by the limited differences in error reduction between the Case A (climatological) and Case B (climatological by water year type) experiments, the strength of this approach lies more in its ability to capture the first-order spatial distribution of bias rather than its second-order interannual variability. Meaning, the historically informed and spatially distributed bias corrections developed herein are an effective tool for downscaling coarse-resolution precipitation input, but less clearly effective at describing its interannual bias.

Results demonstrate that the assimilation of accumulation season snow depth further improves SWE, whereas fSCA assimilation generally does not. fSCA assimilation prior to 1 April more often degrades than improves posterior SWE estimates, due to the weak relationship between fSCA and SWE outside of the ablation season. In contrast, snow depth assimilation before 1 April leads to a 45% reduction of NRSMD in SWE and a 6% increase in R (excluding the special case of water year 2015). In WY 2015, the precipitation forcing does not capture an observed snowfall event after the last-assimilated snow depth observation; neither the seasonally applied precipitation bias correction nor the assimilation is able to rectify this error. We suggest that assimilation of more observations after single-day anomalies like these could help. This underscores how the assimilation of reliable remote-sensing observations can mitigate forcing anomalies in addition to reducing overall bias and uncertainty. Although remotely-sensed snow depth observations such as those taken by ASO are not readily available everywhere, they are proven to be a good source for improvement in SWE estimation on top of bias correction methods.

The improved SWE estimates provide value for snowmelt-driven streamflow predictions, especially in high snow years. We find that using bias-corrected precipitation reduces average bias relative to the Uncorrected baseline in predicted April-July runoff by 46-52% and improves average correlation between daily snowmelt and observed streamflow by 31-39%.

There is the potential for this type of precipitation bias correction in mountain environments everywhere that historical SWE reanalysis datasets have or could be developed, without having to rely on in situ data. It is expected that this type of bias correction be especially useful in regions where historical SWE reanalysis datasets have accurately improved (or are expected to improve) SWE estimates. The power of such an approach lies in the ability to simultaneously downscale and bias-correct globally-available (coarse) precipitation products (e.g., MERRA2 in this work) for use in estimating mountain SWE. The implications of this are widespread. This precipitation bias correction method can lead to improved accuracy of hydrologic models in both research and operational contexts. Because precipitation is a primary driver of hydrologic models, the impact of higher-resolution, higher-accuracy gridded precipitation input is considerable. The value is particularly high in mountainous regions or at elevations with high precipitation uncertainty and/or limited in situ data, which makes other more traditional downscaling methods less applicable.

Future work could also explore alternative sources of prior precipitation, including products that are already downscaled to a finer resolution (i.e., PRISM). Other avenues of investigation could explore more sophisticated methods such as machine learning for bias correction estimation, the assimilation of other sources of real-time snow observations, and the impact of real-time SWE spatial estimates on streamflow forecasts through spatially distributed hydrologic modelling. Of particular relevance to the operational context, another pathway for future work is to explore how the derived bias correction, informed by historical relationships between the b factor and precipitation, snowfall conditions, or other factors, could be updated through the season as more real-time information becomes available.

Data availability

595 The snow water equivalent (SWE) estimates from the modelling and data assimilation experiments and for the historical reference dataset as well as the historical *b* bias correction factors are publicly available at [10.5281/zenodo.14014679](https://doi.org/10.5281/zenodo.14014679). Streamflow observations are available from the California Data Exchange Center (CDEC) at <https://cdec.water.ca.gov>.

Author contribution

600 M.v.K contributed to the development of methodology, funding acquisition, formal analysis, investigation, visualization, and writing. S.M contributed to the conceptualization, funding acquisition, development of methodology, review and editing.

Competing interests

The authors declare that they have no conflict of interest.

Acknowledgments

605 The authors would like to acknowledge and thank Dr. Yiwen Fang and Dr. Yufei Liu for their work in preparing the inputs for and applying the reanalysis framework.

References

Aalstad, K., Westermann, S., Schuler, T. V., Boike, J., and Bertino, L.: Ensemble-based assimilation of fractional snow-covered area satellite retrievals to estimate the snow distribution at Arctic sites, *The Cryosphere*, 12, 247–270, 610 <https://doi.org/10.5194/tc-12-247-2018>, 2018.

Alonso-González, E., Aalstad, K., Baba, M. W., Revuelto, J., López-Moreno, J. I., Fiddes, J., Essery, R., and Gascoin, S.: The Multiple Snow Data Assimilation System (MuSA v1.0), *Geoscientific Model Development*, 15, 9127–9155, <https://doi.org/10.5194/gmd-15-9127-2022>, 2022.

615

Andreadis, K. M. and Lettenmaier, D. P.: Assimilating remotely sensed snow observations into a macroscale hydrology model, *Advances in Water Resources*, 29(6), 872–886, <https://doi.org/10.1016/j.advwatres.2005.08.004>, 2006.

620 Bair, E. H., Abreu Calfa, A., Rittger, K., and Dozier, J.: Using machine learning for real-time estimates of snow water equivalent in the watersheds of Afghanistan, *The Cryosphere*, 12(5), 1579-1594, <https://doi.org/10.5194/tc-12-1579-2018>, 2018.

625 Bair, E. H., Rittger, K., Skiles, S. M., and Dozier, J.: An Examination of Snow Albedo Estimates From MODIS and Their Impact on Snow Water Equivalent Reconstruction, *Water Resources Research*, 55(9), 7826-7842, <https://doi.org/10.1029/2019WR024810>, 2019.

Berg, N. and Hall, A.: Anthropogenic warming impacts on California snowpack during drought, *Geophysical Research Letters*, 44(5), 2511-2518, <https://doi.org/10.1002/2016GL072104>, 2017.

630 Chen, H., Sun, L., Cifelli, R., and Xie, P.: Deep learning for bias correction of satellite retrievals of orographic precipitation, *IEEE Transactions on Geoscience and Remote Sensing*, 60, 1-11, <https://doi.org/10.1109/TGRS.2021.3105438>, 2022.

635 Cho, E., Vuyovich, C. M., Kumar, S. V., Wrzesien, M. L., Kim, R. S., and Jacobs, J. M.: Precipitation biases and snow physics limitations drive the uncertainties in macroscale modeled snow water equivalent, *Hydrology and Earth System Sciences*, 26(22), 5721-5735, <https://doi.org/10.5194/hess-26-5721-2022>, 2022.

640 Clark, M. P., Hendrikx, J., Slater, A. G., Kavetski, D., Anderson, B., Cullen, N. J., Kerr, T., Örn Hreinsson, E., and Woods, R. A.: Representing spatial variability of snow water equivalent in hydrologic and land-surface models: A review, *Water Resources Research*, 47, W07526, <https://doi.org/10.1029/2011WR010745>, 2011

Cortes, G., Girotto, M., and Margulis, S.: Snow process estimation over the extratropical Andes using a data assimilation framework integrating MERRA data and Landsat imagery, *Water Resources Research*, 52(4), 2582-2600, <https://doi.org/10.1002/2015WR018376>, 2016.

645

De Lannoy, G. J. M., Reichle, R. H., Houser, P. R., Arsenault, K. R., Verhoest, N. E. C., and Pauwels, V. R. N.: Satellite-Scale Snow Water Equivalent Assimilation into a High-Resolution Land Surface Model, *Journal of Hydrometeorology*, 11(2), 352-369, <https://doi.org/10.1175/2009JHM1192.1>, 2010.

650 Dozier, J.: Mountain hydrology, snow color, and the fourth paradigm, *Eos, Transactions American Geophysical Union*, 92(43), 373-374, <https://doi.org/10.1029/2011EO430001>, 2011.

Dozier, J., Bair, E. H., and Davis, R. E.: Estimating the spatial distribution of snow water equivalent in the world's mountains: Spatial distribution of snow in the mountains, Wiley Interdisciplinary Reviews: Water, 3(3), 461-655 474, <https://doi.org/10.1002/wat2.1140>, 2016.

Fang, Y., Liu, Y., and Margulis, S. A.: A western United States snow reanalysis dataset over the Landsat era from water years 1985 to 2021, *Scientific Data*, 9(1), 677, <https://doi.org/10.1038/s41597-022-01768-7>, 2022.

660 Fang, Y., Liu, Y., Li, D., Sun, H., and Margulis, S. A.: Spatiotemporal snow water storage uncertainty in the midlatitude American Cordillera, *The Cryosphere*, 17(12), 5175-5195, <https://doi.org/10.5194/tc-17-5175-2023>, 2023.

Giroto, M., Margulis, S. A., and Durand, M.: Probabilistic SWE reanalysis as a generalization of deterministic SWE reconstruction techniques, *Hydrological Processes*, 28(12), 3875-3895, <https://doi.org/10.1002/hyp.9887>, 2014.

665

Gutmann, E., Pruitt, T., Clark, M. P., Brekke, L., Arnold, J. R., Raff, D. A., and Rasmussen, R. M.: An intercomparison of statistical downscaling methods used for water resource assessments in the United States, *Water Resources Research*, 50, 7167-7186, <https://doi.org/10.1002/2014WR015559>, 2014.

670 Hamlet, A. F., Huppert, D., and Lettenmaier, D. P.: Economic Value of Long-Lead Streamflow Forecasts for Columbia River Hydropower, *J. Water Resour. Plann. Manage.*, 128, 91-101, [https://doi.org/10.1061/\(ASCE\)0733-9496\(2002\)128:2\(91\)](https://doi.org/10.1061/(ASCE)0733-9496(2002)128:2(91)), 2002.

675 He, M., Russo, M., and Anderson, M.: Predictability of Seasonal Streamflow in a Changing Climate in the Sierra Nevada, *Climate*, 4(4), 57, <https://doi.org/10.3390/cli4040057>, 2016.

Herbert, J. N., Raleigh, M. S., and Small, E. E.: Reanalyzing the spatial representativeness of snow depth at automated monitoring stations using airborne lidar data, *The Cryosphere*, 18, 3495-3512, <https://doi.org/10.5194/tc-18-3495-2024>, 2024.

680 Koster, R. D., Mahanama, S. P. P., Livneh, B., Lettenmaier, D. P., and Reichle, R. H.: Skill in streamflow forecasts derived from large-scale estimates of soil moisture and snow, *Nature Geoscience*, 3(9), 613-616, <https://doi.org/10.1038/ngeo944>, 2010.

685 Kumar, R., Samaniego, L., and Attinger, S.: Implications of distributed hydrologic model parameterization on water fluxes at multiple scales and locations, *Water Resources Research*, 49, 360-379, <https://doi.org/10.1029/2012WR012195>, 2013.

Largeron, C., Dumont, M., Morin, S., Boone, A., Lafaysse, M., Metref, S., Cosme, E., Jonas, T., Winstral, A., and Margulis, S. A.: Toward snow cover estimation in mountainous areas using modern data assimilation methods: A review, *Frontiers in Earth Science*, 8, 325, <https://doi.org/10.3389/feart.2020.00325>, 2020.

690

Lettenmaier, D. P., Alsdorf, D., Dozier, J., Huffman, G. J., Pan, M., and Wood, E. F.: Inroads of remote sensing into hydrologic science during the WRR era, *Water Resources Research*, 51(9), 7309-7342, <https://doi.org/10.1002/2015WR017616>, 2015.

Li, B., Huang, Y., Du, L., and Wang, D.: Bias correction for precipitation simulated by RegCM4 over the upper reaches of the Yangtze River based on the mixed distribution quantile mapping method, *Atmosphere*, 12, 1566, <https://doi.org/10.3390/atmos12121566>, 2021.

700 Liston, G. E.: Representing Subgrid Snow Cover Heterogeneities in Regional and Global Models, *Journal of Climate*, 17(6), 1381-1397, [https://doi.org/10.1175/1520-0442\(2004\)017<1381>2.0.CO;2](https://doi.org/10.1175/1520-0442(2004)017<1381>2.0.CO;2), 2004.

700

Liu, Y. and Margulis, S. A.: Deriving Bias and Uncertainty in MERRA-2 Snowfall Precipitation Over High Mountain Asia, *Frontiers in Earth Science*, 7, <https://doi.org/10.3389/feart.2019.00280>, 2019.

705 Liu, Y., Fang, Y., and Margulis, S. A.: Spatiotemporal distribution of seasonal snow water equivalent in High Mountain Asia from an 18-year Landsat-MODIS era snow reanalysis dataset, *The Cryosphere*, 15(11), 5261-5280, <https://doi.org/10.5194/tc-15-5261-2021>, 2021.

710

Löber, C., Fayne, J., Hashemi, H., and Smith, L. C.: Bias correction of 20 years of IMERG satellite precipitation data over Canada and Alaska, *Journal of Hydrology: Regional Studies*, 47, 101386, <https://doi.org/10.1016/j.ejrh.2023.101386>, 2023.

710

715 Lu, X. Y., Tang, G. Q., Wang, X. Q., Liu, Y., Wei, M., and Zhang, Y. X.: The development of a two-step merging and downscaling method for satellite precipitation products, *Remote Sensing*, 12, 398, <https://doi.org/10.3390/rs12030398>, 2020. Sharifi, E., Saghafian, B., and Steinacker, R.: Downscaling satellite precipitation estimates with multiple linear regression, artificial neural networks, and spline interpolation techniques, *Journal of Geophysical Research: Atmospheres*, 124, 789–805, <https://doi.org/10.1029/2018JD029241>, 2019.

Ma, Z. Q., He, K., Tan, X., Xu, J. T., Fang, W. Z., He, Y., and Hong, Y.: Comparisons of spatially downscaling TMPA and IMERG over the Tibetan Plateau, *Remote Sensing*, 10, 1883, <https://doi.org/10.3390/rs10121883>, 2018.

720 Magnusson, J., Gustafsson, D., Hüsler, F., and Jonas, T.: Assimilation of point SWE data into a distributed snow cover model comparing two contrasting methods, *Water Resources Research*, 50, 7816–7835, <https://doi.org/10.1002/2014WR015302>, 2014.

725 Margulis, S. A., Girotto, M., Cortes, G., and Durand, M.: A Particle Batch Smoother Approach to Snow Water Equivalent Estimation, *Journal of Hydrometeorology*, 16(4), 1752-1772, <https://doi.org/10.1175/JHM-D-14-0177.1>, 2015.

Margulis, S. A., Cortes, G., Girotto, M., and Durand, M.: A Landsat-Era Sierra Nevada Snow Reanalysis (1985-2015), *Journal of Hydrometeorology*, 17(4), 1203-1221, <https://doi.org/10.1175/JHM-D-15-0177.1>, 2016.

730 Margulis, S. A., Fang, Y., Li, D., Lettenmaier, D. P., & Andreadis, K.: The utility of infrequent snow depth images for deriving continuous space-time estimates of seasonal snow water equivalent, *Geophysical Research Letters*, 46, 5331-5340, <https://doi.org/10.1029/2019GL082507>, 2019.

735 Painter, T. H., Berisford, D. F., Boardman, J. W., Bormann, K. J., Deems, J. S., Gehrke, F., Hedrick, A., Joyce, M., Laidlaw, R., Marks, D., Mattmann, C., McGurk, B., Ramirez, P., Richardson, M., Skiles, S. M., Seidel, F. C., & Winstral, A.: The Airborne Snow Observatory: Fusion of scanning lidar, imaging spectrometer, and physically-based modeling for mapping snow water equivalent and snow albedo, *Remote Sensing of Environment*, 184, 139-152, <https://doi.org/10.1016/j.rse.2016.06.018>, 2016.

740 Pan, M.: Snow process modeling in the North American Land Data Assimilation System (NLDAS): 2. Evaluation of model simulated snow water equivalent, *Journal of Geophysical Research*, 108(D22), <https://doi.org/10.1029/2003JD003994>, 2003.

745 Pflug, J. M., Margulis, S. A., and Lundquist, J. D.: Inferring watershed-scale mean snowfall magnitude and distribution using multidecadal snow reanalysis patterns and snow pillow observations, *Hydrological Processes*, 36, e14581, <https://doi.org/10.1002/hyp.14581>, 2022.

Raleigh, M. S., Lundquist, J. D., and Clark, M. P.: Exploring the impact of forcing error characteristics on physically based snow simulations within a global sensitivity analysis framework, *Hydrology and Earth System Sciences*, 19(7), 3153-3179, <https://doi.org/10.5194/hess-19-3153-2015>, 2015.

750 Schneider, D. and Molotch, N. P.: Real-time estimation of snow water equivalent in the Upper Colorado River Basin using MODIS-based SWE reconstructions and SNOTEL data, *Water Resources Research*, 52(10), 7892-7910, <https://doi.org/10.1002/2016WR019067>, 2016.

755 Schreiner-McGraw, A. P. and Ajami, H.: Impact of Uncertainty in Precipitation Forcing Data Sets on the Hydrologic Budget of an Integrated Hydrologic Model in Mountainous Terrain, *Water Resources Research*, 56(12), e2020WR027639, <https://doi.org/10.1029/2020WR027639>, 2020.

760 Selkowitz, D., Painter, T., Rittger, K., Schmidt, G., and Forster, R.: The USGS Landsat Snow Covered Area Product—Methods and preliminary validation, chap. 5 of Selkowitz, D., Automated approaches for snow and ice cover monitoring using optical remote sensing: Salt Lake City, University of Utah, Ph.D. dissertation, p. 76-119, 2017. [Also available at https://www.researchgate.net/publication/331024289_The_USGS_Landsat_Snow_Covered_Area_Products_Methods_and_Preliminary_Validation]

765 Sun, S. and Xue, Y.: Implementing a new snow scheme in the Simplified Simple Biosphere Model, *Advances in Atmospheric Sciences*, 18(3), 335-354, <https://doi.org/10.1007/BF02919314>, 2001.

770 Tanaka, S. K., Zhu, T., Lund, J. R., Howitt, R. E., Jenkins, M. W., Pulido, M. A., Tauber, M., Ritzema, R. S., and Ferreira, I. C.: Climate warming and water management adaptation for California, *Climatic Change*, 76(3-4), 361-387, <https://doi.org/10.1007/s10584-006-9079-5>, 2006.

775 Velasquez, P., Messmer, M., and Raible, C. C.: A new bias-correction method for precipitation over complex terrain suitable for different climate states: A case study using WRF (version 3.8.1), *Geoscientific Model Development*, 13, 5007–5027, <https://doi.org/10.5194/gmd-13-5007-2020>, 2020.

780 Wang, F., Tian, D., and Carroll, M.: Customized deep learning for precipitation bias correction and downscaling, *Geoscientific Model Development*, 16, 535–556, <https://doi.org/10.5194/gmd-16-535-2023>, 2023.

785 Wood, A. W., Lettenmaier, D. P., & Vail, L. W.: Long-range experimental hydrologic forecasting for the eastern United States, *Journal of Geophysical Research*, 107(D20), 4429, <https://doi.org/10.1029/2001JD000659>, 2002.

Xue, Y., Sun, S., Kahan, D. S., and Jiao, Y.: Impact of parameterizations in snow physics and interface processes on the simulation of snow cover and runoff at several cold region sites, *Journal of Geophysical Research: Atmospheres*, 108(D22), 2002JD003174, <https://doi.org/10.1029/2002JD003174>, 2003.

Yang, K., Musselman, K. N., Rittger, K., Margulis, S. A., Painter, T. H., and Molotch, N. P.: Combining ground-based and remotely sensed snow data in a linear regression model for real-time estimation of snow water equivalent, *Advances in Water Resources*, 160, 104075, <https://doi.org/10.1016/j.advwatres.2021.104075>, 2022.

790 Yoshikane, T., and Yoshimura, K.: A downscaling and bias correction method for climate model ensemble simulations of local-scale hourly precipitation, *Scientific Reports*, 13, 9412, <https://doi.org/10.1038/s41598-023-36489-3>, 2023.

Zhao, N.: An efficient downscaling scheme for high-resolution precipitation estimates over a high mountainous watershed, *Remote Sensing*, 13, 234, <https://doi.org/10.3390/rs13020234>, 2021.

795

Zheng, Z., Molotch, N. P., Oroza, C. A., Conklin, M. H., and Bales, R. C.: Spatial snow water equivalent estimation for mountainous areas using wireless-sensor networks and remote-sensing products, *Remote Sensing of Environment*, 215, 44-56, <https://doi.org/10.1016/j.rse.2018.05.029>, 2018.